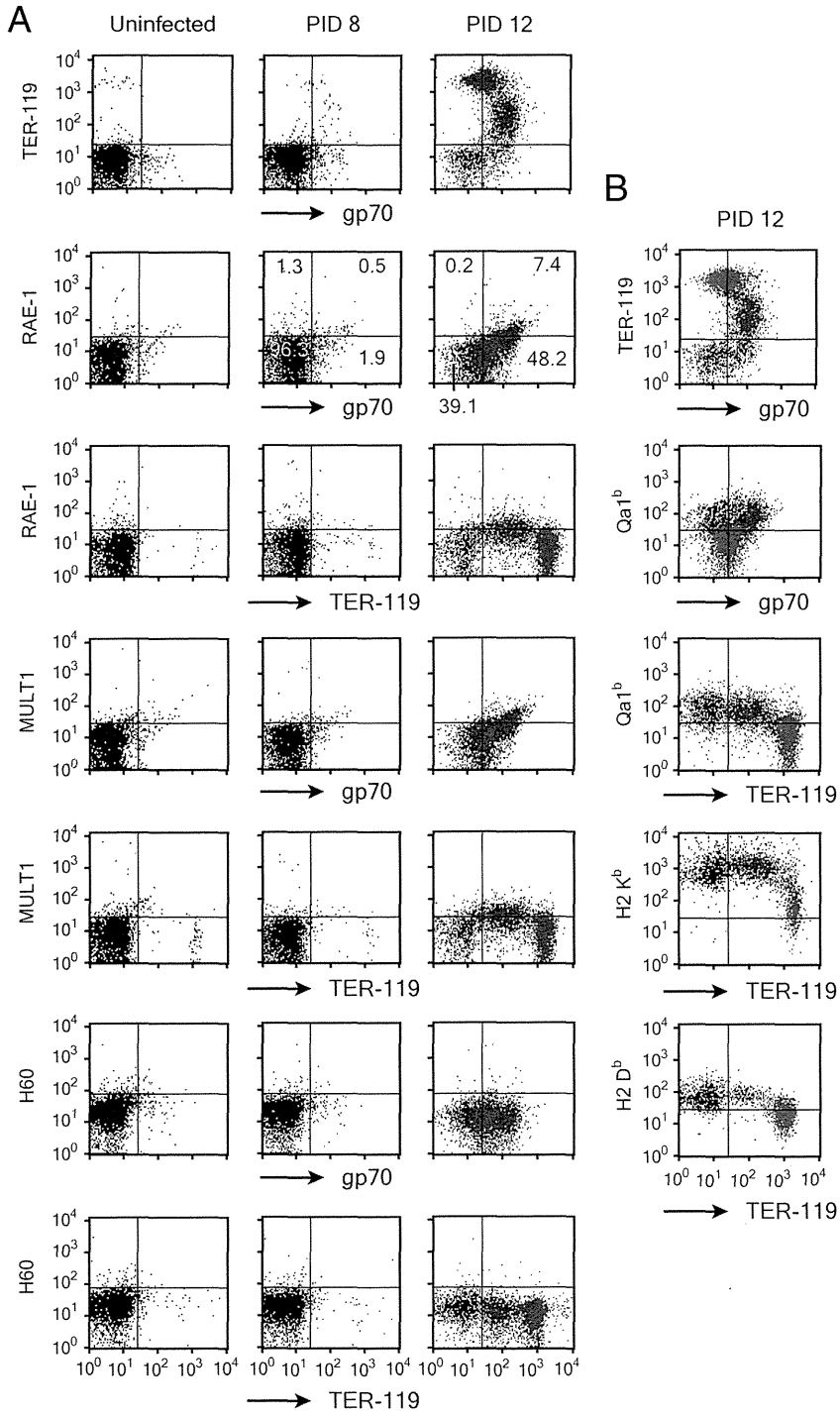

FIG. 3. Representative dot plots showing the expression of NK receptor ligand proteins (A) and MHC class I and class Ib molecules (B) on the surfaces of spleen cells in FV-infected $CB6F_1$ mice. $CB6F_1$ mice were inoculated with 150 SFFU FV, and at least 4 mice were killed at PID 4, 8, and 12 to remove the spleen. Multicolor flow cytometric analyses were performed with each indicated Ab. Uninfected mice were similarly analyzed as controls. Mature erythrocytes and dead cells were excluded by setting a polygonal gate in the dot plots showing intensities of forward scatter and the fluorescence for 7-aminoactinomycin D. Demarcation lines were set based on the fluorescence levels observed by incubating the cells with isotype control Ab. Data on PID 4 are omitted from this figure, as they are essentially similar to those on PID 8, except that $gp70^+$ populations are much smaller. In the middle and right panels of the second row of dot plots in panel A, the number in each quadrant represents the percentage of cells that expressed the indicated markers above or below the level of the corresponding demarcation line. Patterns observed with all 4 mice at each time point were consistent with those shown here. In panel A, purple dots, TER-119^{Lo} $gp70^{Hi}$ cells; red dots, TER-119^{Hi} $gp70^+$ erythroblasts. In panel B, red dots, TER-119^{Lo} $gp70^{Hi}$ cells; pink dots, TER-119^{Hi} $gp70^+$ erythroblasts.

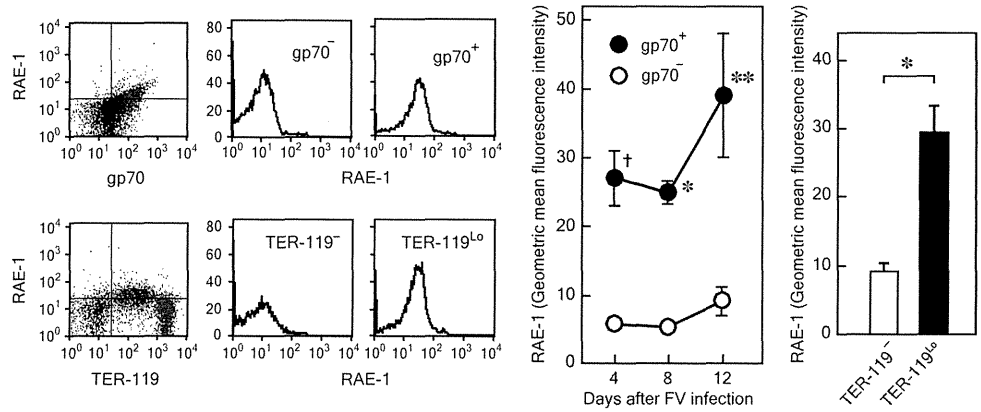

FIG. 4. Different levels of RAE-1 expression between viral gp70-positive and -negative spleen cells in mice infected with FV. $CB6F_1$ mice were inoculated with 150 SFFU of LDV-free FV, and multicolor flow cytometric analyses were performed on nucleated cells as described for Fig. 3. Representative dot plots and histograms on the left show different levels of RAE-1 expression on pairs of $gp70^-$ and $gp70^+$ or $TER\text{-}119^-$ and $TER\text{-}119^{Lo}$ populations at PID 12. $TER\text{-}119^-$ and $TER\text{-}119^{Lo}$ populations are those shown with black and purple dots, respectively, in Fig. 3A. Changes in averages of geometric mean fluorescence intensity (GMFI) for RAE-1 among $gp70^-$ and $gp70^+$ cells after FV infection are shown in the middle panel. GMFI were calculated by using the region statistics function of the CellQuest software. Each datum shown here is the mean ± SEM. calculated with GMFI data obtained from 4 mice. Differences between $gp70^+$ and $gp70^-$ populations were examined by two-way ANOVA with Bonferroni *post hoc* tests: *, $P < 0.05$; †, $P < 0.01$; **, $P < 0.001$. The right panel shows averages of GMFI for RAE-1 compared between the $TER\text{-}119^-$ and $TER\text{-}119^{Lo}$ populations at PID 12. Each bar shows mean ± SEM calculated with GMFI data obtained from 4 or 5 mice. *, $P < 0.02$, by paired t test.

by the Ab injections in the above depletion experiments, as activated T cells are known to express asialoGM1 in some viral infections (41). To further demonstrate the direct involvement of the RAE-1 ligand and NKG2D receptor in confining the early expansion of FV-infected cells, blocking Abs were administered to infected $CB6F_1$ mice. The numbers of FV-producing cells in the spleen significantly increased in the animals that were given either NKG2D- or RAE-1-blocking Ab in comparison with those in the control mice (Fig. 5A and D). Further, in the presence of the RAE-1-blocking Ab, FV-infected $CB6F_1$ mice showed significantly larger spleen sizes than control mice (Fig. 5E), confirming that FV-infected erythroid progenitor cells are recognized and their expansion is regulated through NKG2D–RAE-1 interactions *in vivo*. As the effects of the NKG2D or RAE-1 blockade were observed at as early as PID 6, prior to the expansion of $NKG2D^+$ $CD8^+$ T cells (Fig. 1B), it is most likely that mainly $NKG2D^+$ NK cells were responsible for the above early confinement of FV-induced erythroid cell proliferation.

Increased expression of RAE-1 depends on retroviral replication rather than on erythroid cell proliferation. As the FV complex induces massive proliferation and terminal differentiation of erythroid progenitor cells in mice possessing the *Fv2*^{s} allele, the above-described increase in RAE-1 expression on $TER\text{-}119^{Lo}$ cells may depend on the specific differentiation stage (proerythroblasts and early basophilic erythroblasts) or activated status of red cell precursors, rather than on FV infection. To examine this, we first induced an increased erythropoiesis by administering phenylhydrazine (PHZ) instead of FV infection. After administration of PHZ, both the $TER\text{-}119^{Lo}$ and $TER\text{-}119^{Hi}$ populations became discernible in the spleens of $CB6F_1$ mice; however, neither population in PHZ-treated mice showed increased expression of RAE-1, unlike the $gp70^+$ $TER\text{-}119^{Lo}$ population in FV-infected mice (Fig. 6A). Similar results were also obtained for MULT1. Thus, the increase in RAE-1 and MULT1 expression on the $TER\text{-}119^{Lo}$ population was likely caused by FV infection, not by induced erythropoiesis.

To further elucidate putative relationships between FV replication and RAE-1 expression on target cells of FV infection, mice deficient of either of the FV resistance factors APOBEC3 and BAFF-R, which show markedly enhanced FV replication and exaggerated pathology (46, 47), were examined. Mice of the *Fv2*$^{r/r}$ background were utilized so that the effects of FV replication on RAE-1 expression could be further separated from those of SFFV-induced erythroid cell proliferation. Both APOBEC3- and BAFF-R-deficient mice showed markedly increased numbers of gp70-expressing cells in the spleen in comparison with those in the wild-type (WT) animals (Fig. 6B). Importantly, RAE-1-positive cells increased in association with the increased numbers of $gp70^+$ cells in APOBEC3- and BAFF-R-deficient animals. In APOBEC3-deficient mice, most of the $gp70^+$ cells were $TER\text{-}119^+$ and $B220^-$, and these cells showed increased expression of RAE-1 proteins on their surfaces (Fig. 6B, arrows). In mice deficient of BAFF-R, even larger numbers of both $TER\text{-}119^+$ (Fig. 6B, orange dots) and $TER\text{-}119^-$ cells (Fig. 6B, red dots) were infected with FV, and these $gp70^+$ cells expressed higher levels of RAE-1 than $gp70^-$ cells. Interestingly, in FV-infected *BAFF-R*$^{-/-}$ mice a significant proportion of $B220^+$ B lymphocytes were also infected with FV, and they expressed higher levels of RAE-1 than uninfected B cells (Fig. 6B, blue dots).

As SFFV-induced growth potentiation of erythroid cells is limited in the above-described *Fv2*^{r} B6-background mice and as $gp70^+$ B cells, as well as erythroid cells, expressed higher levels of RAE-1 proteins than $gp70^-$ cells, the above results suggested that the replication of F-MuLV alone in the absence of SFFV might induce increased RAE-1 expression on target cells. Thus, we next infected the same gene-targeted animals with an infectious molecular clone of F-MuLV. In APOBEC3-

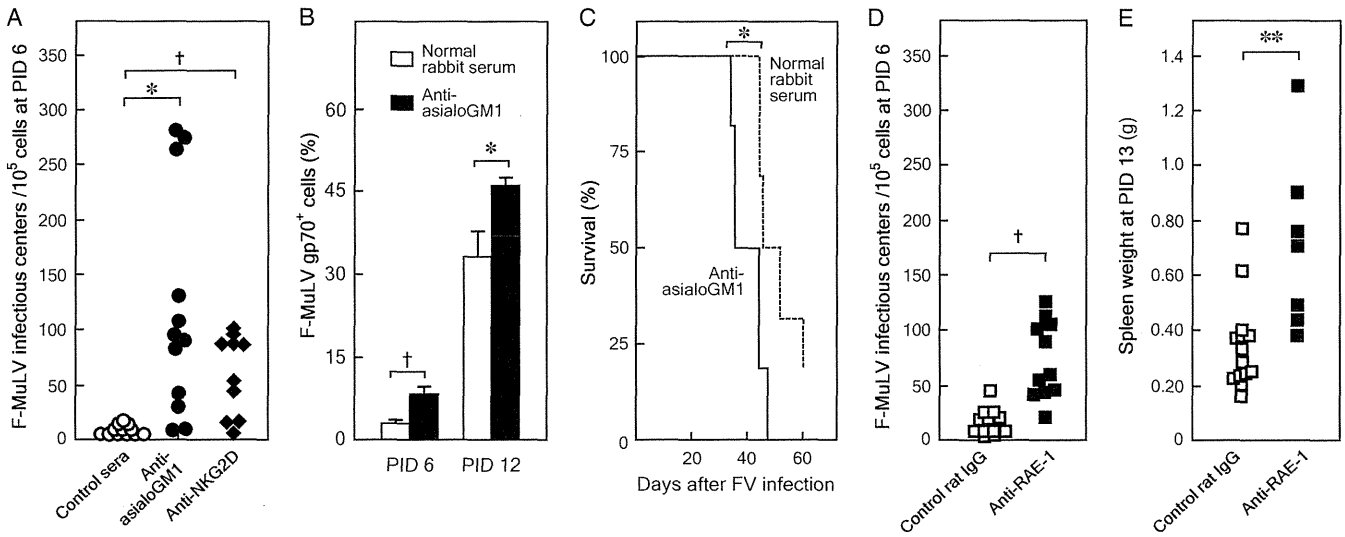

FIG. 5. Effects of the administration of anti-asialoGM1, anti-NKG2D, or anti-RAE-1 Ab on the expansion of virus-producing cells in the spleen and the development of FV-induced pathologies. (A) $CB6F_1$ mice were injected with either the anti-asialoGM1 or the blocking anti-NKG2D Ab and inoculated with 150 SFFU of FV. Control mice were injected with a mixture of normal rabbit and normal rat sera (control sera), and similarly infected. F-MuLV infectious centers in the spleen were enumerated by fluorescent focus assays as described previously (19, 44–47). Each symbol represents a datum from an individual mouse. As the anti-asialoGM1 and anti-NKG2D Ab-injected groups were compared with the common control group given the mixture of unimmunized sera, Bonferroni's correction was performed for multiple comparisons: *, $P = 0.0028 < \alpha(0.05) = 0.0253$; †, $P < 0.0005 < \alpha(0.05) = 0.0253$ by Welch's t test. (B) $CB6F_1$ mice were injected with the anti-asialoGM1 Ab as described previously (16) and inoculated with 150 SFFU of FV. Percentages of NK cells expressing both DX5 and NK-1.1 markers among spleen cells were monitored by multicolor flow cytometry as shown in Fig. 1, inset, and percentages of $gp70^+$ cells were determined by the specific binding of Ab 720 at the indicated time points. Data shown here are mean ± SEM calculated with values obtained from 5 to 12 animals per group at each time point. Comparisons were made between the anti-asialoGM1-treated and control groups: *, $P < 0.03$; †, $P < 0.005$ by Welch's t test. (C) Survival of anti-asialoGM1-treated animals ($n = 6$) after FV infection compared with that of control mice given normal rabbit serum ($n = 6$). As $CB6F_1$ mice are highly susceptible to FV and most died within 60 days after inoculation with as low as 15 SFFU in a previous experiment (16), a slightly lower dose of 50 SFFU was selected here in an attempt to detect the possibly increased susceptibility in NK-depleted mice. Two survival curves were compared by Mantel-Cox log-rank test: *, $P = 0.026$. (D and E) Groups of $CB6F_1$ mice were injected with either the RAE-1-bloking Ab (49) or control rat IgG and inoculated with 150 (D) or 50 SFFU (E) of FV. Spleen infectious centers were enumerated at PID 6 as described previously (19, 44–47), separate groups were killed at PID 13, and their spleen weights measured. The slightly reduced dose was utilized for the experiment shown in panel E, for the sake of consistency with the survival experiment described in the legend to panel C. Each symbol represents a datum from an individual mouse. †, $P < 0.0005$ by Welch's t test; **, $P = 0.0028$ by Student's t test.

deficient mice, a large proportion of $TER\text{-}119^+$ cells were infected and expressed gp70; however, unlike the $TER\text{-}119^+$ $gp70^+$ cells in the same gene-targeted mice infected with FV complex, these cells showed only a slight increase in RAE-1 expression (Fig. 7A, arrows). Similar effects of the absence of the SFFV component on the expression of RAE-1 in erythroid cells were more evidently observed with BAFF-R-deficient mice: $TER\text{-}119^+$ cells were infected with F-MuLV and expressed gp70, but unlike the same population of erythroid cells in FV-infected mice, these cells did not show a marked increase in the expression of RAE-1 proteins on their surfaces (Fig. 7A, orange dots). On the other hand, $B220^+$ B cells in F-MuLV-infected *BAFF-R*$^{-/-}$ mice (Fig. 7A, blue dots) showed increased expression of RAE-1 as observed upon FV infection.

To further confirm the above differences in RAE-1 expression levels between erythroid cells and B lymphocytes upon FV and F-MuLV infections, $TER\text{-}119^+$ and $B220^+$ cells were gated and their expression levels of RAE-1 proteins were compared between $gp70^+$ and $gp70^-$ populations. When infected with the FV complex, the $gp70^+$ populations of both $TER\text{-}119^+$ and $B220^+$ cells expressed significantly higher levels of RAE-1 than the corresponding $gp70^-$ cells in both APOBEC3- and BAFF-R-deficient animals (Fig. 7B). The average levels of RAE-1 expression on $gp70^+$ cells were 2.69 ± 0.12 and 3.28 ± 0.26 times higher than those on $gp70^-$ cells among $TER\text{-}119^+$ and $B220^+$ cell populations, respectively, in FV-infected BAFF-R-deficient mice. On the other hand, although levels of RAE-1 expression between $gp70^+$ and $gp70^-$ populations were significantly different, $gp70^+$ cells among $TER\text{-}119^+$ erythroid cells in F-MuLV-infected BAFF-R-deficient mice expressed on their surfaces a level of RAE-1 proteins only 1.47 ± 0.06 times higher than that of $gp70^-$ cells, while RAE-1 expression in the $gp70^+$ population of $B220^+$ B lymphocytes became even higher than that observed with FV-infected mice. In fact, the average level of RAE-1 expression on $gp70^+$ cells among $B220^+$ cells was 4.54 ± 0.13 times higher than that on $gp70^-$ cells. Thus, these results indicate that SFFV is required for highly increased expression of RAE-1 on $TER\text{-}119^+$ erythroid cells, while replication of F-MuLV alone induces increased RAE-1 expression in $B220^+$ B cells.

DISCUSSION

As we have shown here, $NKG2D^+$ NK cells expanded in the spleen and the levels of RAE-1 expression became preferentially higher on the surfaces of viral gp70-expressing cells in FV-infected mice. Although we have not tested all known

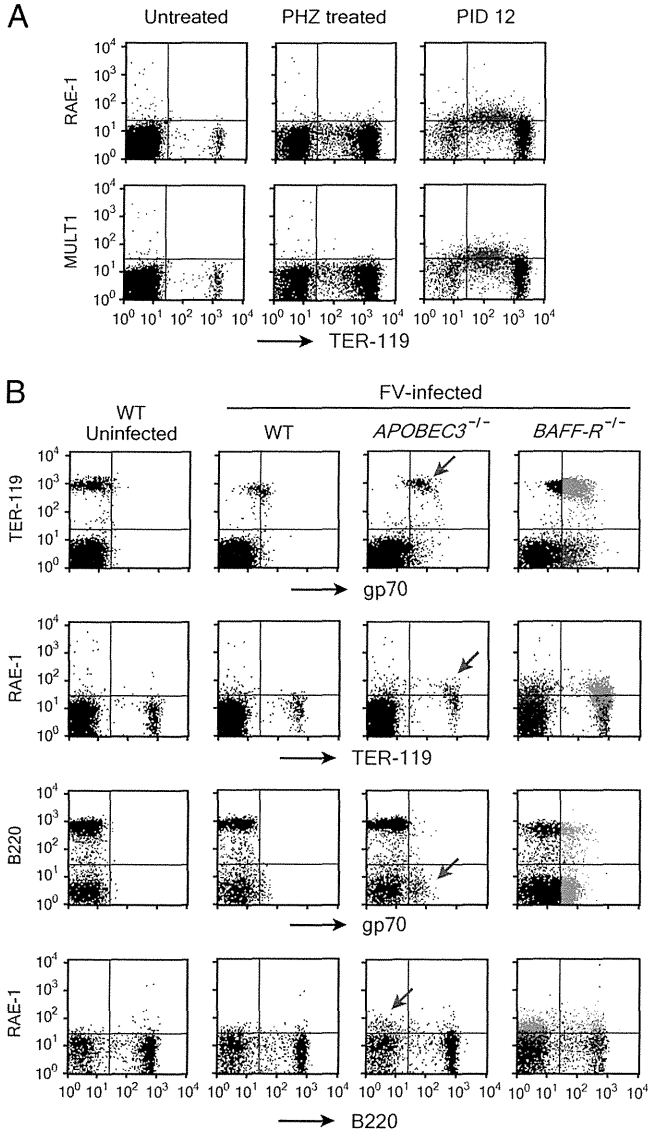

FIG. 6. RAE-1 expression on erythroid progenitor cells is induced by FV infection, not by erythropoiesis. (A) Representative dot plots showing the expression of NK receptor ligand proteins on the surfaces of nucleated spleen cells in phenylhydrazine-treated $CB6F_1$ mice. $CB6F_1$ mice were either injected with 1.2 mg/mouse PHZ on days 0 and 1 or inoculated with 150 SFFU FV on day 0, and at least 4 mice were killed on day 5 or day 12, respectively, to remove the spleen. Multicolor flow cytometric analyses were performed on nucleated cells with each indicated Ab. Demarcation lines were set based on the fluorescence levels observed by incubating the cells with isotype control Ab. Patterns observed with all 4 mice for each experimental group were consistent with those shown here. (B) Representative dot plots showing the expression of viral gp70, RAE-1, erythroid marker TER-119, and B-cell marker B220 on the surfaces of nucleated spleen cells in FV-infected B6 mice lacking an FV-resistance factor. As *Fv2*$^{r/r}$ mice were utilized, they were infected with 5×10^4 SFFU of FV complex, and 4 to 5 mice for each group were killed to remove the spleen. Flow cytometric analyses were performed as described in the legend to Fig. 3. Representative data obtained at PID 10 are shown here. In panel A, red dots, TER-119^{Lo} gp70^{Hi} cells. In panel B, red dots, TER-119$^-$ gp70$^+$ cells; orange dots, TER-119$^+$ gp70$^+$ cells; purple dots, B220$^-$ gp70$^+$ cells; blue dots, B220$^+$ gp70$^+$ cells in FV-infected *BAFF-R*$^{-/-}$ mice.

ligands for NK cell receptors, the nearly complete abrogation of the killing activities against F-MuLV-induced FBL-3 target cells exerted by DX5$^+$ cells purified from FV-infected $CB6F_1$ mice *in vitro* and the significant increase in the number of FV infectious centers *in vivo* in the presence of the NKG2D-blocking Ab clearly indicate that the NKG2D receptor is involved primarily in the recognition and elimination of infected erythroid cells in FV-inoculated animals. Further, although the levels of induction of RAE-1 proteins on the surfaces of gp70$^+$ erythroid cells were relatively low, as detectable by flow cytometry with the currently utilized Ab, and the same gp70$^+$ TER-119^{Lo} cells retained Qa-1^b molecules on their surfaces, the induced RAE-1 proteins are apparently sufficient to induce the elimination of FV-infected erythroid cells *in vivo*, as the administration of the RAE-1-blocking Ab resulted in significantly increased numbers of infectious centers and more pronounced splenomegaly after FV inoculation. In this regard, FBL-3 cells were killed efficiently by purified NK cells despite their expression of Qa-1^b on the surfaces. Thus, NKG2D–RAE-1 interactions are involved in the elimination of virus-infected cells in the early stages of FV infection *in vivo*. These results are consistent with the previous finding that overexpression of VEGF-A paradoxically resulted in delayed development of FV-induced leukemia, probably due partly to enhanced NK cell activities in the transgenic mice (4).

The mechanisms by which FV infection upregulates the expression of RAE-1 molecules in erythroid progenitor cells and B lymphocytes are currently unknown. Several cytokines, including IFN-γ, have been shown to upregulate the expression of these retinoid-inducible genes (8, 49), and we have demonstrated in the present study that IFN-γ augments the expression of *Raet1* genes in F-MuLV-induced leukemia cells. As the production of IFN-γ in the spleens of FV-infected mice has been detected at as early as 5 days after virus inoculation (31), the induction of *Raet1* gene expression in FV-infected cells might be mediated by IFN-γ. However, as higher levels of RAE-1 proteins were expressed preferentially on gp70$^+$ cells, it is unlikely that cytokine-mediated induction, which should work on both FV-infected and uninfected cells in the spleen, is responsible mainly for the increased levels of RAE-1 protein expression on FV-infected cells. The lack of increased RAE-1 expression on TER-119^{Lo} cells in PHZ-injected mice also indicates the presence of a virus-specific, rather than a differentiation- or growth-associated, mechanism of RAE-1 induction. In this regard, infection of mouse primary B lymphocytes with highly leukemogenic Abelson MuLV induces the expression of activation-induced cytidine deaminase (AID), and the genotoxic action of AID leads to upregulation of NKG2D ligands on infected cell surfaces (11). HIV-1 Vpr is also known to upregulate the expression of NKG2D ligands on cell surfaces (35), and the above Vpr-induced upregulation of NKG2D ligand expression has been shown to be mediated through the DNA damage response (48). Thus, it is tempting to speculate that repeated proviral integrations into the erythroid progenitor cells that are facilitated in the presence of SFFV-induced growth potentiation may cause DNA damage and the resultant upregulation of RAE-1 expression in FV-infected erythroid cells.

Taking advantage of known FV-resistant host factors (5, 12, 25, 27, 46, 47), we successfully dissected here the effect of

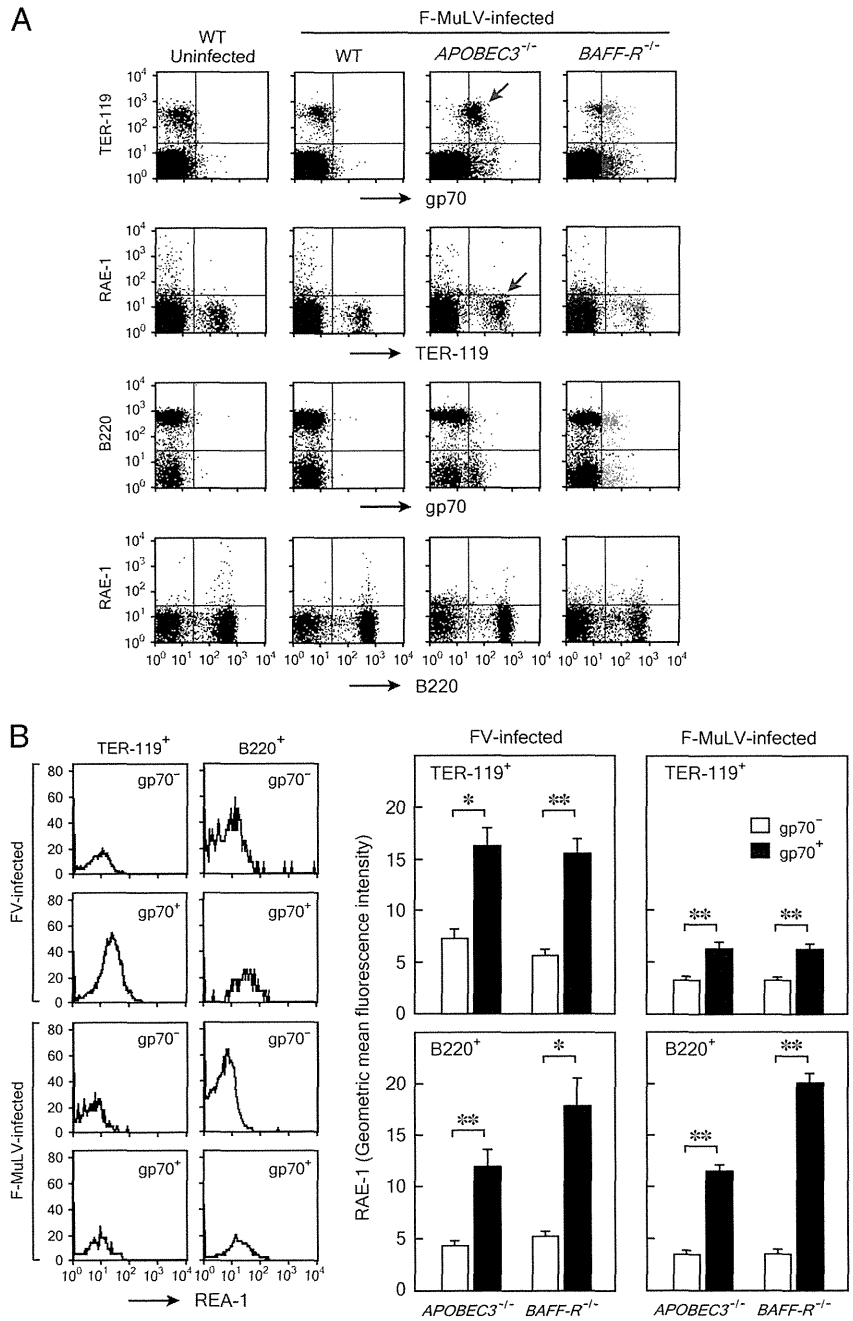

FIG. 7. RAE-1 expression on spleen cells upon infection with F-MuLV alone. (A) Representative dot plots showing the expression of viral gp70, RAE-1 proteins, TER-119, and B220 on the surfaces of nucleated spleen cells in F-MuLV-infected B6 mice lacking an FV resistance factor. Mice were infected with 5×10^4 fluorescent focus units of F-MuLV (FB-29), and 4 or 5 mice for each group were killed to remove the spleen. Flow cytometric analyses were performed as described for Fig. 3. Representative data obtained at PID 10 are shown here. Arrows, slight increase in RAE-1 expression on the surfaces of TER-119$^+$ gp70$^+$ cells in F-MuLV-infected *APOBEC3*$^{-/-}$ mice. Red dots, TER-119$^-$ gp70$^+$ cells; orange dots, TER-119$^+$ gp70$^+$ cells; purple dots, B220$^-$ gp70$^+$ cells; blue dots, B220$^+$ gp70$^+$ cells in F-MuLV-infected *BAFF-R*$^{-/-}$ mice. (B) Representative histograms on the left show different levels of RAE-1 expression on gp70$^-$ and gp70$^+$ populations of TER-119$^+$ erythroid and B220$^+$ B cells. Averages of GMFI for RAE-1 compared between the gp70$^-$ and gp70$^+$ populations of TER-119$^+$ erythroid cells and B220$^+$ B lymphocytes are shown on the right. Each bar shows mean ± SEM calculated with GMFI data obtained from 4 or 5 mice. *, $P < 0.02$; **, $P < 0.004$ by paired *t* test.

SFFV-induced erythroid cell growth potentiation from that of FV replication on RAE-1 induction in target cells. In fact, FV infection in the absence of massive erythroid cell proliferation still resulted in highly increased RAE-1 expression on TER-119$^+$ erythroid cells in *Fv2*^{r} B6 mice lacking either APOBEC3 or BAFF-R. Highly increased expression of RAE-1 on infected erythroid as well as B cells in the gene-targeted B6 mice indicates a close correlation between high levels of retroviral rep-

lication and induction of RAE-1 expression on target cells. It should be noted, however, that although B cells expressed similarly increased levels of RAE-1 proteins upon infection with FV complex or with F-MuLV alone, levels of RAE-1 induction on erythroid cells became much higher in the presence of the SFFV component. Thus, in the above conditions of nonrestricted retroviral replication, F-MuLV alone can induce RAE-1 expression in B cells, while SFFV is also required for the induction of high levels of RAE-1 in erythroid cells. In fact, SFFV-induced growth potentiation of infected erythroid cells in the *Fv2*^{s}-possessing $CB6F_1$ mice further enhanced RAE-1 expression on gp70$^+$ erythroblasts, as RAE-1 levels on gp70$^+$ cells in $CB6F_1$ mice were apparently higher than those in the gene-targeted B6 mice (compare fluorescence intensities between Fig. 4 and 7). Nevertheless, the above cell type-associated differences in RAE-1 expression in F-MuLV-infected B6 mice may facilitate further dissection of viral and cellular factors that are involved in retrovirus-induced RAE-1 upregulation.

In the present study, we observed a lag in the increase of TER-119$^+$ erythroblasts until PID 8, followed by an abrupt and massive increase of gp70$^+$ cells in the spleen by PID 12. An abrupt increase in the number of TER-119$^+$ cells in the spleen starting around PID 8 has repeatedly been observed with *Fv2*^{s}-possessing mice (16, 19, 26), which is consistent with a recent finding of two distinctive populations of target cells for FV infection (43). Thus, one population expresses the short-form STK and generates erythropoietin-independent erythroid burst-forming units (BFU-E) in the bone marrow soon after FV infection, while cells of the other population migrate into the spleen as infectious centers, interact with the stromal cells to express bone morphogenic protein 4, and cause the expansion of stress BFU-E. It is tempting to speculate that the cells expressing increased levels of RAE-1 and MULT1 are FV-infected stress BFU-E and that they are susceptible to NK killing. As the depletion of NK cells or the blockade of either NKG2D or RAE-1 resulted in significantly increased FV infectious centers in the spleen at as early as PID 6, followed by significantly more pronounced splenomegaly and earlier death, it is also possible that NK cells are restricting the migration of CD31$^+$ Kit$^+$ CD41$^+$ Sca1$^-$ Lin$^-$ infectious center cells into the spleen. In fact, immunization of mice with the gp70-derived Th-cell epitope suppressed the above abrupt expansion of TER-119$^+$ cells in the spleen that otherwise started from PID 8 (16, 19, and 26), and this vaccine effect was abrogated by depletion of NK cells (16), indicating that Th cell-mediated activation of NK cells may have suppressed the migration of FV infectious centers from bone marrow. Thus, this model may also shed light on basic mechanisms through which the migration of committed erythroid progenitor cells from bone marrow to the spleen might be regulated by NK cell functions.

ACKNOWLEDGMENTS

This work was supported in part by grants-in-aid from the Ministry of Education, Culture, Sports, Science, and Technology of Japan, including the High-Tech Research Center, Medico-Technical Cooperation, and Anti-Aging Center grants, those from the Ministry of Health, Labor, and Welfare of Japan for Research on HIV/AIDS, and those from the Japan Health Sciences Foundation. The use of radioisotopes, animal experiments, and flow cytometric analyses were supported by members of the Central Research Facilities, Kinki University School of Medicine.

We are grateful to J. Brian Dowell for critically reading and correcting the manuscript and to Yoshiko Ito, Department of Respiratory Medicine and Allergology, Kinki University School of Medicine, for her help in operating the AutoMACS.

REFERENCES

1. **Alter, G., et al.** 2007. Evolution of innate and adaptive effector cell functions during acute HIV-1 infection. J. Infect. Dis. **195:**1452–1460.
2. **Arase, H., T. Saito, J. H. Phillips, and L. L. Lanier.** 2001. Cutting edge: the mouse NK cell-associated antigen recognized by DX5 monoclonal antibody is CD49b (α_2 integrin, very late antigen-2). J. Immunol. **167:**1141–1144.
3. **Azakami, K., et al.** 2009. Severe loss of invariant NKT cells exhibiting anti-HTLV-1 activity in patients with HTLV-1-associated disorders. Blood **114:**3208–3215.
4. **Cervi, D., et al.** 2007. Enhanced natural-killer cell and erythropoietic activities in VEGF-A-overexpressing mice delay F-MuLV-induced erythroleukemia. Blood **109:**2139–2146.
5. **Chesebro, B., M. Miyazawa, and W. J. Britt.** 1990. Host genetic control of spontaneous and induced immunity to Friend murine retrovirus infection. Annu. Rev. Immunol. **8:**477–499.
6. **Costello, R. T., C. Fauriat, S. Sinori, E. Marcenaro, and D. Olive.** 2004. NK cells: innate immunity against hematopoietic malignancies? Trends Immunol. **26:**328–333.
7. **Dittmer, U., et al.** 2001. Role of interleukin-4 (IL-4), IL-12, and gamma interferon in primary and vaccine-primed immune responses to Friend retroviral infection. J. Virol. **75:**654–660.
8. **Faria, P. A., et al.** 2005. VSV disrupts the Rae1/mrnp41 mRNA nuclear export pathway. Mol. Cell **17:**93–102.
9. **Gaudieri, S., et al.** 2005. Killer immunoglobulin-like receptors and HLA act both independently and synergistically to modify HIV disease progression. Genes Immun. **6:**683–690.
10. **Giavedoni, L. D., M. C. Velasquillo, L. M. Parodi, G. B. Hubbard, and V. L. Hodora.** 2000. Cytokine expression, natural killer cell activation, and phenotypic changes in lymphoid cells from rhesus macaques during acute infection with pathogenic simian immunodeficiency virus. J. Virol. **74:**1648–1657.
11. **Gourzi, P., T. Leonova, and F. N. Papavasiliou.** 2006. A role for activation-induced cytidine deaminase in the host response against a transforming retrovirus. Immunity **24:**779–786.
12. **Hasenkrug, K. J., and B. Chesebro.** 1997. Immunity to retroviral infection: the Friend virus model. Proc. Natl. Acad. Sci. U. S. A. **94:**7811–7816.
13. **Ho, E. L., et al.** 2002. Costimulation of multiple NK cell activation receptors by NKG2D. J. Immunol. **169:**3667–3675.
14. **Howcroft, T. K., and D. S. Singer.** 2003. Expression of nonclassical MHC class Ib genes: comparison of regulatory elements. Immunol. Res. **27:**1–30.
15. **Iannello, A., O. Debbeche, S. Samarani, and A. Ahmad.** 2008. Antiviral NK cell responses in HIV infection. I. NK cell receptor genes as determinants of HIV resistance and progression to AIDS. J. Leuko. Biol. **84:**1–26.
16. **Iwanami, N., A. Niwa, Y. Yasutomi, N. Tabata, and M. Miyazawa.** 2001. Role of natural killer cells in resistance against Friend retrovirus-induced leukemia. J. Virol. **75:**3152–3163.
17. **Jamieson, A. M., et al.** 2002. The role of the NKG2D immunoreceptor in immune cell activation and natural killing. Immunity **17:**19–29.
18. **Kabat, D.** 1989. Molecular biology of Friend viral erythroleukemia. Curr. Top. Microbiol. Immunol. **148:**1–42.
19. **Kawabata, H., et al.** 2006. Peptide-induced immune protection of CD8$^+$ T cell-deficient mice against Friend retrovirus-induced disease. Int. Immunol. **18:**183–198.
20. **Kina, T., et al.** 2000. The monoclonal antibody TER-119 recognizes a molecule associated with glycophorin A and specifically marks the late stages of murine erythroid lineage. Br. J. Haematol. **109:**280–287.
21. **Kottilil, S., et al.** 2003. Innate immunity in human immunodeficiency virus infection: effect of viremia on natural killer cell function. J. Infect. Dis. **187:**1038–1045.
22. **Maier, L. M., et al.** 2008. NKG2D–RAE-1 receptor-ligand variation does not account for the NK cell defect in Nonobese diabetic mice. J. Immunol. **181:**7073–7080.
23. **Martin, M. P., et al.** 2002. Epistatic interaction between KIR3DS1 and HLA-B delays the progression to AIDS. Nat. Genet. **31:**429–434.
24. **Martin, M. P., et al.** 2007. Innate partnership of HLA-B and KIR3DL1 subtypes against HIV-1. Nat. Genet. **39:**733–740.
25. **Miyazawa, M.** 2004. Host genes that influence immune and non-immune resistance mechanisms against retroviral infections. Rec. Res. Dev. Virol. **6:**105–118.
26. **Miyazawa, M., et al.** 1995. Immunization with a single T helper cell epitope abrogates Friend virus-induced early erythroid proliferation and prevents late leukemia development. J. Immunol. **155:**748–758.
27. **Miyazawa, M., S. Tsuji-Kawahara, and Y. Kanari.** 2008. Host genetic factors that control immune responses to retrovirus infections. Vaccine **26:**2981–2996.

28. **Ney, P. A., and A. D. D'Andrea.** 2000. Friend erythroleukemia revisited. Blood **96:**3675–3680.
29. **Ogasawara, K., et al.** 2004. NKG2D blockade prevents autoimmune diabetes in NOD mice. Immunity **20:**757–767.
30. **Ogasawara, K., and L. L. Lanier.** 2005. NKG2D in NK and T cell-mediated immunity. J. Clin. Immunol. **25:**534–540.
31. **Peterson, K. E., M. Iwashiro, K. J. Hasenkrug, and B. Chesebro.** 2000. Major histocompatibility complex class I gene controls the generation of gamma interferon-producing $CD4^+$ and $CD8^+$ T cells important for recovery from Friend retrovirus-induced leukemia. J. Virol. **74:**5363–5367.
32. **Peterson, K. E., I. Stromnes, R. Messer, K. Hasenkrug, and B. Chesebro.** 2002. Novel role of $CD8^+$ T cells and major histocompatibility complex class I genes in the generation of protective $CD4^+$ Th1 responses during retrovirus infection in mice. J. Virol. **76:**7942–7948.
33. **Pradet-Balade, B., C. Leberbauer, N. Schweifer, and F. Boulmé.** 2010. Massive translational repression of gene expression during mouse erythroid differentiation. Biochim. Biophys. Acta **1799:**630–641.
34. **Ravet, S., et al.** 2007. Distinctive NK-cell receptor repertoires sustain high-level constitutive NK-cell activation in HIV-exposed uninfected individuals. Blood **109:**4296–4305.
35. **Richard, J., S. Sindhu, T. N. Pham, J. P. Belzile, and E. A. Cohen.** 2010. HIV-1 Vpr up-regulates expression of ligands for the activating NKG2D receptor and promotes NK cell-mediated killing. Blood **115:**1354–1363.
36. **Robertson, M. N., et al.** 1991. Production of monoclonal antibodies reactive with a denatured form of the Friend murine leukemia virus gp70 envelope protein: use in a focal infectivity assay, immunohistochemical studies, electron microscopy and Western blotting. J. Virol. Methods **34:**255–271.
37. **Sasaki, Y., S. Casola, J. L. Kutok, K. Rajewsky, and M. Schmidt-Supprian.** 2004. TNF family member B cell-activating factor (BAFF) receptor-dependent and -independent roles for BAFF in B cell physiology. J. Immunol. **173:**2245–2252.
38. **Scott-Algara, D., et al.** 2003. Increased NK cell activity in HIV-1-exposed but uninfected Vietnamese intravenous drug users. J. Immunol. **171:**5663–5667.
39. **Seaman, W. E.** 2000. Natural killer cells and natural killer T cells. Arthritis Rheum. **43:**1204–1217.
40. **Sieff, C., et al.** 1982. Changes in cell surface antigen expression during hemopoietic differentiation. Blood **60:**703–713.
41. **Slifka, M. K., R. R. Pagarigan, and J. L. Whitton.** 2000. NK markers are expressed on a high percentage of virus-specific $CD8^+$ and $CD4^+$ T cells. J. Immunol. **164:**2009–2015.
42. **Stromnes, I. M., et al.** 2002. Temporal effects of gamma interferon deficiency on the course of Friend retrovirus infection in mice. J. Virol. **76:**2225–2232.
43. **Subramanian, A., et al.** 2008. Friend virus utilizes the BMP4-dependent stress erythropoiesis pathway to induce erythroleukemia. J. Virol. **82:**382–393.
44. **Sugahara, D., S. Tsuji-Kawahara, and M. Miyazawa.** 2004. Identification of a protective $CD4^+$ T-cell epitope in $p15^{gag}$ of Friend murine leukemia virus and role of the MA protein targeting the plasma membrane in immunogenicity. J. Virol. **78:**6322–6334.
45. **Takamura, S., et al.** 2010. Premature terminal exhaustion of Friend virus-specific effector $CD8^+$ T cells by rapid induction of multiple inhibitory receptors. J. Immunol. **184:**4696–4707.
46. **Takeda, E., et al.** 2008. Mouse APOBEC3 restricts Friend leukemia virus infection and pathogenesis in vivo. J. Virol. **82:**10998–11008.
47. **Tsuji-Kawahara, S., et al.** 2010. Persistence of viremia and production of neutralizing antibodies differentially regulated by polymorphic *APOBEC3* and *BAFF-R* loci in Friend virus-infected mice. J. Virol. **84:**6082–6095.
48. **Ward, J., et al.** 2009. HIV-1 Vpr triggers natural killer cell-mediated lysis of infected cells through activation of the ATR-mediated DNA damage response. PLoS Pathog. **5:**e1000613.
49. **Yokoyama, W. M., and B. F. M. Plougastel.** 2003. Immune functions encoded by the natural killer gene complex. Nat. Rev. Immunol. **3:**304–316.
50. **Zhang, J., M. Socolovsky, A. W. Gross, and H. F. Lodish.** 2003. Role of Ras signaling in erythroid differentiation of mouse fetal liver cells: functional analysis by a flow cytometry-based novel culture system. Blood **102:**3938–3946.
51. **Zhou, R., H. Wei, R. Sun, J. Zhang, and Z. Tian.** 2007. NKG2D recognition mediates Toll-like receptor 3 signaling-induced breakdown of epithelial homeostasis in the small intestines of mice. Proc. Natl. Acad. Sci. U. S. A. **104:**7512–7515.

An Evolutionary Analysis of *RAC2* Identifies Haplotypes Associated with Human Autoimmune Diseases

Manuela Sironi,†,[1] Franca Rosa Guerini,†,[2] Cristina Agliardi,[2] Mara Biasin,[3] Rachele Cagliani,[1] Matteo Fumagalli,[1] Domenico Caputo,[2] Andrea Cassinotti,[4] Sandro Ardizzone,[4] Milena Zanzottera,[2] Elisabetta Bolognesi,[2] Stefania Riva,[1] Yasuyoshi Kanari,[5] Masaaki Miyazawa,[5] and Mario Clerici,*[,2,6]

[1]Bioinformatics Laboratory, Scientific Institute IRCCS E. Medea, Bosisio Parini (LC), Italy

[2]Don C. Gnocchi Foundation ONLUS, IRCCS, Milan, Italy

[3]Department of Clinical Science, LITA Vialba, University of Milan, Milan, Italy

[4]Department of Clinical Sciences, Chair of Gastroenterology, Luigi Sacco University Hospital, Milan, Italy

[5]Department of Immunology, Kinki University School of Medicine, Osaka-Sayama, Osaka, Japan

[6]Department of Biomedical Sciences and Technologies LITA Segrate, University of Milan, Milan, Italy

†These authors contributed equally to this work.

***Corresponding author:** E-mail: mario.clerici@unimi.it.

Associate editor: Willie Swanson

Abstract

The human *RAC2* gene encodes a small GTP-binding protein with a pivotal role in immune activation and in the induction of peripheral immune tolerance through restimulation-induced cell death (RICD). Different human pathogens target the protein product of *RAC2*, suggesting that the gene may be subject to natural selection, and that variants in *RAC2* may affect immunological phenotypes in humans. We scanned the genomic region encompassing the entire transcription unit for the presence of putative noncoding regulatory elements conserved across mammals. This information was used to select two *RAC2* gene regions and analyze their intraspecific genetic diversity. Results suggest that a region covering the 3′ untranslated region has been a target of multiallelic balancing selection (or diversifying selection), and three major *RAC2* haplogroups occur in human populations. Haplotypes belonging to one of these clades are associated with increased susceptibility to multiple sclerosis ($P = 0.022$) and earlier onset of disease symptoms ($P = 0.025$). This same haplogroup is significantly more common in patients with Crohn's disease compared with healthy controls ($P = 0.048$). These data reinforce recent evidences that susceptibility alleles/haplotypes are shared among multiple autoimmune disorders and support a causal "role for *RAC2*" variants in the pathogenesis of autoimmune diseases. Other genes with a role in RICD have previously been associated with autoimmunity in humans, suggesting that this pathway and RAC2 may represent novel therapeutic targets in autoimmune disorders.

Key words: *RAC2*, balancing selection, haplotype, multiple sclerosis, Crohn's disease.

Introduction

The human *RAC2* (ras-related C3 botulinum toxin substrate 2) gene encodes a member of the Ras superfamily of GTP-binding proteins primarily expressed in cells of hematopoietic origin (reviewed in Heasman and Ridley 2008). The protein product of *RAC2* regulates several processes central to immune and inflammatory responses including proliferation of primary T cells and differentiation towards the Th1 subtype, dendritic cell migration, neutrophil nicotinamide adenine dinucleotide phosphatase oxidase activity, and B cell maturation (Knaus et al. 1991; Li et al. 2000, 2002; Kim and Dinauer 2001; Yu et al. 2001; Croker et al. 2002; Benvenuti et al. 2004; Decoursey and Ligeti 2005). Therefore, *RAC2* can be regarded as a pivotal gene in the elicitation of immune responses, but it also plays a role in the induction of peripheral immune tolerance. Indeed, RAC2 represents an essential component of restimulation-induced cell death (RICD) via the Fas/FasL pathway (Ramaswamy et al. 2007).

Genes involved in immune response are believed to be frequent targets of natural selection (reviewed in Hurst 2009; Barreiro and Quintana-Murci 2010); in particular, balancing selection, which is thought to be a relatively rare phenomenon in humans (Asthana et al. 2005; Charlesworth 2006), has targeted a few genes involved in both innate and adaptive immunity (Ferrer-Admetlla et al. 2008; Barreiro and Quintana-Murci 2010; Sironi and Clerici 2010). This observation has been explained by the need to finely tune effective responses to pathogens on one side and development of pathogenic autoimmune/inflammatory reactions on the other (Ferrer-Admetlla et al. 2008). Yet, the role of autoimmunity and chronic inflammatory diseases as selective pressure during the course of human evolutionary history remains to be evaluated. Therefore, the maintenance of susceptibility alleles for autoimmune diseases may also be regarded as a possible by-product of adaptation to pathogen exposure (reviewed

in Sironi and Clerici 2010). In line with this view, susceptibility alleles for several human diseases have been shown to have increased in frequency in human populations as a result of recent positive selection (Barreiro and Quintana-Murci 2010), and several alleles that predispose to inflammatory bowel disease (IBD) have been a target of pathogen-driven selection (Fumagalli, Pozzali, et al. 2009). These observations suggest that past selective pressures exerted by infectious agents might have contributed to shaping the frequency spectrum of susceptibility alleles for autoimmune diseases.

Irrespective of the underlying mechanisms responsible for the maintenance of genetic diversity in humans, the identification of genes/gene regions subjected to natural selection can provide relevant information for the identification of functional variants that may influence complex phenotypic traits.

Here, we integrated the analysis of inter- and intraspecies genetic diversity to analyze the evolutionary pattern of *RAC2* and demonstrate its role as a susceptibility gene for multiple sclerosis (MS) and Crohn's disease (CD).

Materials and Methods

Analysis of Functional Elements and Sequence Conservation

Data concerning DNaseI hypersensitive sites in CD4+ T cells derive from a previous work (Boyle et al. 2008) and were retrieved from the University of California–San Cruz (UCSC) annotation tables (http://genome.ucsc.edu, Duke DNaseI HS track). PhastCons elements were derived from the UCSC website (tracks: phastConsElements44wayPlacMamm and phastConsElements44wayPrimates). Only conserved elements longer than 15 bp were considered. Similarly, information on histone marks was obtained from UCSC annotation tracks (ENCODE Integrated Regulation Tracks).

HapMap Samples and Sequencing

Human genomic DNA for the three human HapMap populations (Europeans, CEU; Yoruba, YRI; and Asian, AS) was obtained from the Coriell Institute for Medical Research. The two regions in *RAC2* were polymerase chain reaction (PCR) amplified and directly sequenced; primer sequences are available upon request. PCR products were treated with ExoSAP-IT (USB Corporation, Cleveland, OH), directly sequenced on both strands with a Big Dye Terminator sequencing Kit (v3.1, Applied Biosystems, Foster City, CA) and run on an Applied Biosystems ABI 3130 XL Genetic Analyzer (Applied Biosystems). Sequences were assembled using AutoAssembler version 1.4.0 (Applied Biosystems) and inspected manually by two distinct operators.

Patients, Controls, and Genotyping

For the MS case/control association study, a total of 722 individuals were enrolled: 387 relapsing-remitting multiple sclerosis (RRMS) patients (266 females and 121 males) and 335 age- and sex-matched healthy individuals (206 females and 129 males) of the same geographic origin (collection site). All patients and controls were Italians of Caucasian ethnicity. The RRMS patients were followed by MS Center of Don Gnocchi Foundation in Milan, Italy. Median age was 41.9 ± 10.9 and 42.32 ± 22.05 years for RRMS and controls, respectively. All patients underwent a standard battery of examinations, including medical history, physical and neurological examination, screening laboratory test, and brain magnetic resonance imaging. All patients with MS fulfilled the McDonald's criteria (McDonald et al. 2001). As for the CD case/control study, we recruited 313 individuals: 149 suffering from CD (96 males and 53 females) and 164 age- and sex-matched healthy individuals (104 males and 60 females). All subjects were Italians of Caucasian ethnicity. Patients referred since diagnosis to the IBD Unit of the Luigi Sacco Hospital in Milano, a third level center for the management of IBD patients, were enrolled. The diagnosis of CD was based on international published criteria, according to clinical, endoscopic, histological, and/or radiological data (Lennard-Jones 1989). A detailed clinical history, as well as laboratory and instrumental diagnostic data, were collected.

This study was designed and carried out in accordance with the Helsinki Declaration. Only patients signing an informed consent form were enrolled in the study, which was approved by the institutional review board.

All RRMS subjects were genotyped for the *HLA-DRB1* locus by sequence-specific primed PCR using Histo Type DNA well plates (BAG, Formedic diagnostici, Milan, Italy).

Genomic DNA was used as template for PCR amplification using TaqMan probes specifically designed to perform a single nucleotide polymorphism (SNP) genotyping assay for rs2899284 (A/G) and rs739041 (A/G) (TaqMan SNP genotyping assay; Applied Biosystems) and using the allelic discrimination real-time PCR method. The PCR consisted of a hot start at 95 °C for 10 min followed by 40 cycles of 94 °C for 15 s and 60 °C for 1 min. Fluorescence detection took place at a temperature of 60 °C. All assays were performed in 10 μl reactions, using TaqMan Genotyping Master Mix on 96-well plates using an ABI 7000 instrument (Applied Biosystems). After Bonferroni correction, the two SNPs complied to Hardy–Weinberg equilibrium (HWE) in all cohorts.

As for the 15 null SNPs used to test for population structure, TaqMan SNP genotyping assays were also used with the same conditions detailed above. The dbSNP IDs and reported minor allele frequencies in CEU were as follows: rs10113320 (0.319), rs10488619 (0.42), rs10785952 (0.363), rs12313915 (0.332), rs12618959 (0.283), rs2220858 (0.362), rs2625956 (0.164), rs2842063 (0.159), rs310644 (0.111), rs6687440 (0.347), rs289816 (0.111), rs4783432 (0.161), rs6001728 (0.221), rs16877243 (0.192), rs1885167 (0.204). All SNPs were in HWE in both RRMS and control subjects.

Population Genetic Analysis

Tajima's *D* (Tajima 1989) and Fu and Li's *D** and *F** (Fu and Li 1993) statistics, as well as diversity parameters θ_w (Watterson 1975) and π (Nei and Li 1979), were calculated using "libsequence" (Thornton 2003), a C++ class library

providing an object-oriented framework for the analysis of molecular population genetic data. Calibrated coalescent simulations were performed using the "cosi" package (Schaffner et al. 2005) and its best-fit parameters for YRI, CEU, and AS populations with 10,000 iterations. Additional coalescent simulations were computed with the ms software (Hudson 2002) specifying the number of chromosomes; the mutation parameter estimated from the data and the recombination rate with 10,000 iterations for each demographic model. The other parameters for each model were set as previously proposed (Marth et al. 2004; Voight et al. 2005). The maximum likelihood ratio Hudson–Kreitman–Aguadé (MLHKA) test was performed using the MLHKA software (Wright and Charlesworth 2004), as previously proposed (Fumagalli, Cagliani, et al. 2009). Briefly, 16 reference loci were randomly selected among National Institute of Environmental Health Sciences (NIEHS) loci shorter than 20 kb that have been resequenced in the three populations; the only criterion was that Tajima's *D* statistic did not suggest the action of natural selection (i.e., Tajima's *D* statistic is higher than the 5th and lower than the 95th percentiles in the distribution of NIEHS genes). The reference set was accounted for by the following genes: *VNN3* (MIM 606592), *PLA2G2D* (MIM 605630), *MB* (MIM 160000), *MAD2L2* (MIM 604094), *HRAS* (MIM 190020), *CYP17A1* (MIM 609300), *ATOX1* (MIM 602270), *BNIP3* (MIM 603293), *CDC20* (MIM 603618), *NGB* (MIM 605304), *TUBA1* (MIM 191110), *MT3* (MIM 139255), *NUDT1* (MIM 600312), *PRDX5* (MIM 606583), *RETN* (MIM 605565), and *JUND* (MIM 165162). In all analyses, the chimpanzee was used as the outgroup.

Data Retrieval, Haplotype Construction, and TMRCA Calculation

Genotype data for 238 resequenced human genes were derived from the NIEHS SNPs Program Web site. In particular, we selected genes that had been resequenced in populations of defined ethnicity including CEU, YUI, and AS (NIEHS panel 2).

For HapMap samples, haplotypes were inferred using PHASE version 2.1 (Stephens et al. 2001; Stephens and Scheet 2005), a program for reconstructing haplotypes from unrelated genotype data through a Bayesian statistical method. Haplotypes for individuals resequenced in this study are available as supplementary table S1, Supplementary Material online.

The median-joining network was constructed using NETWORK 4.5 (Bandelt et al. 1999). Estimate of the time to the most recent common ancestor (TMRCA) was obtained using a maximum likelihood coalescent method implemented in GENETREE (Griffiths and Tavare 1994, 1995). The mutation rate μ was obtained on the basis of the divergence between human and chimpanzee, and under the assumption both that the species separation occurred 6 Ma (Glazko and Nei 2003) and of a generation time of 25 years. Using this μ, a maximum likelihood estimate of θ (θ_{ML}) of 8 was obtained, resulting in an estimated effective population size (N_e) of 16,260, a value comparable to most figures reported in the literature (Tishkoff and Verrelli 2003). With these assumptions, the coalescence time, scaled in $2N_e$ units, was converted into years. For the coalescence process, 10^6 simulations were performed.

Estimates of allelic richness and private allelic richness for the three observed haplogroups were derived via Monte Carlo simulations by applying a rarefaction procedure to account for differences in sample size among clades (Kalinowski 2004). Specifically, we performed 1,000 simulations by randomly drawing g chromosomes (with $g = 20$) without replacement within each haplogroup and counting the number of polymorphic variants and private alleles within each clade. The average number of polymorphisms and private variants in the simulated samples represents our estimate of allelic richness and private allelic richness.

Association Analysis and Population Structure

Haplotype association analysis was performed using PLINK (Purcell et al. 2007) by logistic regression. Haplotype probabilities of individual subjects were incorporated as covariates in the regression models, which estimate the odds ratios associated with having a specific haplotype under an additive model. Sex was also used as a covariate. Wald tests were used to calculate *P* values.

In order to test for the presence of population stratification, 15 "null" SNPs (IDs are reported above) were selected. Specifically, 15 SNPs from a panel of ancestry informative markers (Enoch et al. 2006) were selected to be located on different chromosomes and for having a minor allele frequency in HapMap CEU > 0.10. Using these data, the inflation factor λ (Devlin et al. 2001) was calculated through the use of the Genomic Control (GC) function in the SNPassoc R package (Gonzalez et al. 2007). For estimation of the ancestry proportion for each RRMS and control subject, we used STRUCTURE 2.1 (Pritchard et al. 2000; Falush et al. 2003) based on the genotype information of the 15 null SNPs. Simulation parameters were set to 100,000 burn-ins followed by 100,000 runs. The most common criterion to detect the true number of populations (K) is based on computing an estimate of the posterior probability of the data for a given K, L(K). However, choosing K which maximizes the value of L(K) tends to overestimate the true number of populations, especially when a correction for the correlated population allele frequencies is adopted (Evanno et al. 2005). To overcome this issue, we computed a statistics based on the second rate of change of L(K) with respect to the value of K, as previously proposed (Evanno et al. 2005). The peak of this new function detects the most likely value of K, which, in our case, was estimated to be equal to 2. Individual admixture estimates obtained from STRUCTURE 2.1 were added as continuous covariates (with haplotypes and sex) in a second logistic regression analysis to correct for possible cryptic substructure. Only 1 of the 2 ($K = 2$) admixture proportions was included because the two proportions sum to 1, making them collinear.

For analysis of association between specific *RAC2* haplotypes and age at onset, linear regression analyses were

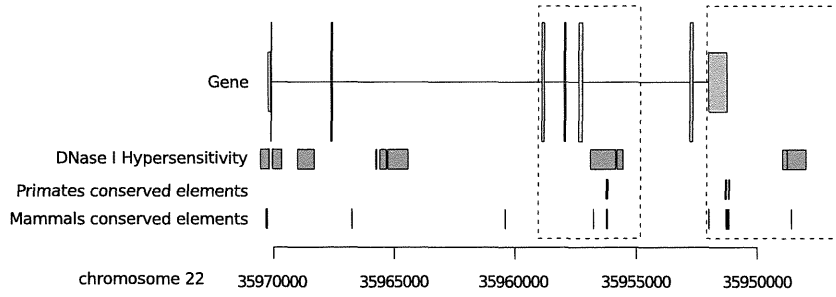

FIG. 1. Schematic diagram of the exon–intron structure of *RAC2*. Along the gene, gray boxes represent exons (coding regions and UTRs are denoted by having different height). The location of DNaseI hypersensitive sites in CD4+ T cells is shown below the gene diagram (green boxes). Noncoding conserved elements in primate (red) and placental mammals (blue) are also reported. The two regions selected for resequencing are delimited by the hatched lines.

performed using PLINK (Purcell et al. 2007). For RRMS subjects, presence/absence of the *HLA-DRB*15* allele was used a covariate in the regression.

Results

Analysis of Interspecies Sequence Conservation

Given the central role of RAC2 in immune responses, it is conceivable that variants located within or in proximity of the gene affect the susceptibility to infectious or autoimmune diseases in humans. If this were the case, such variants may also represent natural selection targets.

No nonsynonymous SNP in the gene has been described in dbSNP (Build 131, http://www.ncbi.nlm.nih.gov/projects/SNP); similarly, inspection of the 1000 Genomes Project data (http://browser.1000genomes.org) identified no amino acid replacement variant, suggesting that protein sequence variation in RAC2 does not contribute significantly to intraspecific and phenotypic diversity in human populations. Therefore, we aimed at identifying *RAC2* genic regions that may be more likely to harbor noncoding functional elements and, possibly, regulatory variants.

To this purpose, we relied on the concept whereby noncoding elements that are conserved across multiple species are more likely to be functional (Sironi et al. 2005). We scanned a genomic region covering the whole RAC2 transcription unit and flanking regions for the presence of DNaseI hypersensitive sites in CD4+ T cells, noncoding regions conserved in placental mammals, and noncoding sequences conserved across primates (see Materials and Methods for details). As reported in figure 1, two distinct regions displayed more than one conserved element and DNaseI hypersensitive sites: One is located in intron 5 and the other covers the 3′ untranslated region and a genomic portion downstream the transcription end site. We therefore selected these two regions, hereafter referred to as $RAC2_{in5}$ (4,202 bp) and $RAC2_{3'}$ (5,560 bp), for further analysis.

Nucleotide Diversity, Neutrality Tests, and Time Estimate

In order to get a complete view of the genetic diversity in $RAC2_{in5}$ and $RAC2_{3'}$, and analyze their evolutionary pattern in humans, we resequenced the two regions in three HapMap populations, namely YRI, CEU, and AS.

Overall, only one coding SNP was identified (Lys84Lys). For both regions, we calculated nucleotide diversity by means of two indexes: θ_w (Watterson 1975), an estimate of the expected per site heterozygosity, and π (Nei and Li 1979), the average number of pairwise sequence nucleotide differences. In order to compare the values we obtained for the two *RAC2* regions, we calculated θ_w and π for 5 kb regions deriving from 238 genes resequenced by the NIEHS program in the same population samples; the percentile rank corresponding to $RAC2_{in5}$ and $RAC2_{3'}$ in the distribution of values for NIEHS genes is reported in table 1 and indicates that $RAC2_{3'}$ displays extremely high nucleotide diversity in all populations; conversely, no exceptional values are observed for $RAC2_{in5}$. These data suggest that genetic diversity in the $RAC2_{3'}$ region might be maintained in human populations by a selective process (e.g., balancing selection).

Under neutral evolution, values of θ_w and π are expected to be roughly equal; for $RAC2_{3'}$, this is not verified, π being higher than θ_w in YRI and CEU (table 1). Tajima's *D* statistic (D_T) (Tajima 1989) was specifically developed to evaluate departure from neutrality by comparing θ_w and π; positive values of D_T indicate an excess of intermediate frequency variants and are a hallmark of balancing selection. Similarly to D_T, Fu and Li's F^* and D^* are based on SNP frequency spectra, but they also take into account whether mutations occur in external or internal branches of a genealogy (Fu and Li 1993). As population history, in addition to selective processes, is known to affect the site frequency spectrum (SFS) and all related statistics, we performed coalescent simulations using a population genetics model that incorporates demographic scenarios (Schaffner et al. 2005). As an empirical comparison, we also exploited the availability of 5 kb windows to obtain a reference distribution of SFS-based statistics in the three populations. Neutrality tests for $RAC2_{3'}$ suggested departure from neutrality in all populations with significantly positive values for at least one statistic in YRI and AS (table 1). In line with these results, the value of D_T in YRI and Fu and Li's D^* in AS were higher than the 95th percentile calculated over the distribution of NIEHS 5 kb windows. Conversely, no departure from

Table 1. Nucleotide Diversity and Summary Statistics.

Region	Pop.[a]	S^b	θ_w ($\times 10^{-4}$)		π ($\times 10^{-4}$)		Tajima's *D* Statistic			Fu and Li's *D**			Fu and Li's *F**		
			Rank		Rank		Rank		*P*	Rank		*P*	Rank		*P*
$RAC2_{in5}$ (4,202 bp)	YRI	21	11.75	0.78	13.89	0.93	0.61	0.90	0.085	0.021	0.66	0.38	0.26	0.75	0.24
	CEU	14	7.83	0.78	11.00	0.87	1.28	0.87	0.079	−0.28	0.47	0.41	0.27	0.62	0.37
	AS	14	7.83	0.82	10.01	0.86	0.88	0.77	0.22	0.17	0.65	0.43	0.47	0.70	0.34
$RAC2_{3'}$ (5,560 bp)	YRI	53	22.38	0.99	27.41	0.99	0.80	0.95	0.032	0.72	0.90	0.052	0.89	0.94	0.028
	CEU	42	17.74	0.98	23.51	0.99	1.15	0.83	0.11	0.95	0.85	0.10	1.21	0.90	0.073
	AS	39	16.47	0.99	15.84	0.95	−0.14	0.47	0.39	1.66	>0.99	0.0038	1.23	0.91	0.086

[a] Population.
[b] Number of segregating sites.

neutrality was observed for $RAC2_{in5}$ (table 1). Coalescent simulations using different demographic models (Marth et al. 2004; Voight et al. 2005) yielded very similar results and are available as supplementary table S2, Supplementary Material online.

In order to further explore the possibility that nucleotide diversity at the $RAC2_{3'}$ region has been maintained by selection, we applied an MLHKA by comparing polymorphisms and divergence levels at $RAC2_{in5}$ and $RAC2_{3'}$ with 16 NIEHS genes resequenced in the three populations we analyzed (see Materials and Methods). Under neutral evolution, the amount of within-species diversity is predicted to correlate with levels of between-species divergence since both depend on the neutral mutation rate (Kimura 1983). The MLHKA test (Wright and Charlesworth 2004) is commonly used to verify this expectation. Results are shown in table 2 and indicate that for $RAC2_{3'}$, a significant excess of polymorphisms compared with divergence is observed in all populations. Conversely, no deviations from neutral expectations was observed for the $RAC2_{in5}$ region (with only borderline significance in YRI).

Under a balancing selection regime, polymorphisms may be maintained in populations for a time, which is longer than expected under neutrality. We used GENETREE to estimate the TMRCA of the $RAC2_{3'}$ haplotype genealogy. The method is based on a maximum likelihood coalescent analysis (Griffiths and Tavare 1994, 1995) and assumes an infinite-site model without recombination. Therefore, haplotypes and sites that violate these assumptions need to be removed. Given the relatively low recombination rate in the region, only nine single segregating sites had to be removed. The resulting gene tree, rooted using the chimpanzee sequence, is partitioned into two deep clades, with clade A further divided into two minor branches (fig. 2) (clades A1 and A2). Using this method, the TMRCA of the whole genealogy amounted to 2.54 My (standard deviation: 0.374 My), whereas the two subclades (A1 and A2) have a shallower TMRCA of around 1.1 My.

Table 2. MLHKA Test.

Region	Fixed Sub[a]	MLHKA					
		YRI		CEU		AS	
		k^b	*P*	k^b	*P*	k^b	*P*
$RAC2_{in5}$	30	2.35	0.048	2.24	0.13	2.25	0.89
$RAC2_{3'}$	59	3.24	2.6×10^{-3}	3.72	4.0×10^{-4}	3.50	8.6×10^{-4}

[a] Number of fixed substitutions (human/chimpanzee).
[b] Selection parameter ($k > 1$ indicates an excess of polymorphism relative to divergence).

Haplotype Analysis and Association with Autoimmune Diseases

In order to gain insight into the distribution of *RAC2* haplotypes in human populations, we constructed a median-joining network (Bandelt et al. 1999) using all variants identified in $RAC2_{in5}$ and $RAC2_{3'}$ with the exclusion of singletons (fig. 3). The topology largely recapitulates the one obtained using GENETREE with two major clades (A and B), and haplotypes in clade A subdivided into two further haplogroups (referred to as A1 and A2) (fig. 3). There are clear differences in the distribution of *RAC2* haplotypes among the three populations we analyzed, although F_{st} values (Wright 1950) were not exceptional compared with those calculated for 5 kb reference windows (supplementary table S3, Supplementary Material online). Estimates of allelic richness (and private allelic richness) within haplogroups were calculated using a rarefaction procedure (Kalinowski 2004) to account for different haplogroup frequency; results indicated that haplogroup A2 had the lowest genetic diversity among the three haplotype clades, whereas B haplotype tended to have high allelic richness (supplementary table S4, Supplementary Material online).

The pivotal role of *RAC2* in immune response led us to verify whether the three major haplogroups were differentially represented when healthy controls were compared with subjects suffering from autoimmune diseases such as MS and CD, two diseases with a strong genetic basis (Weng et al. 2007; Nielsen et al. 2008; Langer-Gould et al. 2010) that suggests the presence of shared genetic determinants.

We selected two variants: rs2899284, located along the major branch separating clades A and B, and rs739041 that identifies haplogroup A1 (fig. 3). The typing of these two variants allows unequivocal haplogroup inference in European populations, as they are nonrecurrent in the phylogeny. The allele frequency of rs2899284 (T) and rs739041 (C) in the three populations we analyzed were as follows: CEU, 0.22 and 0.45; YRI, 0.27 and 0.67; and AS, 0.10 and 0.30.

The two SNPs were genotyped in 387 patients with RRMS and in 149 subjects suffering from CD; two independent cohorts of sex- and aged-matched controls were also

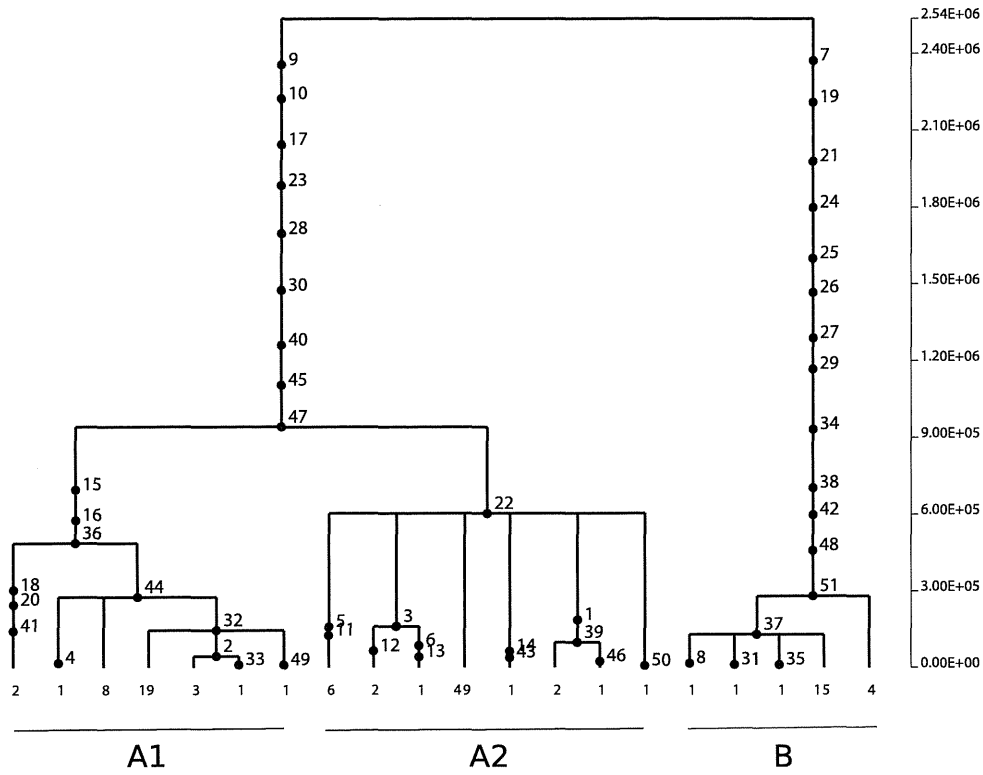

FIG. 2. Estimated haplotype tree for the $RAC2_{3'}$ gene region. Mutations are represented as black dots and named for their physical position along the regions. The absolute frequency of each haplotype is reported.

analyzed. Using logistic regression analysis, haplotypes belonging to haplogroup B resulted to be significantly associated to disease status in both the RRMS and CD case/control studies (table 3).

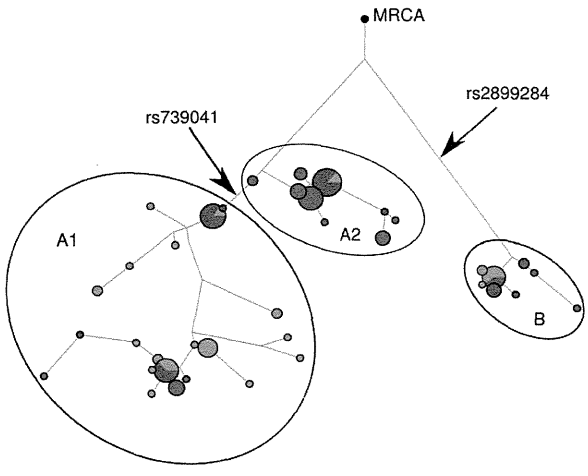

FIG. 3. Median-joining network of *RAC2* haplotypes. Each node represents a different haplotype, with the size of the circle proportional to frequency. Branch lengths are proportional to the number of nucleotide differences. Circles are color coded according to population (green: YRI, blue: CEU, and red: AS). The most recent common ancestor (MRCA) also shown (black circle). The three major haplogroups are evidenced, as well as the position of the two SNPs genotypes in patients and controls.

Although we did not expect substantial levels of population structure in our cohorts as all subjects were Italians with Caucasian ancestry, we verified that the results we obtained are not secondary to cryptic substructure. To this aim, we genotyped RRMS subjects and controls for 15 null SNPs (see Materials and Methods). This procedure was not performed for CD patients as additional genetic material was unavailable. We used null SNPs to apply the GC method (Devlin et al. 2001): Calculation of the inflation parameter λ resulted in a value of 0.92, suggesting that there is no substantial stratification in our samples. Yet, the GC method may not be conservative when few markers are used (Balding 2006). Thus, we used the program STRUCTURE 2.1 (Pritchard et al. 2000; Falush et al. 2003) and included the inferred ancestry proportions of individual cases and controls as continuous covariates in the logistic regression analysis. A significant result was again obtained for haplotypes belonging to haplogroup B.

We next verified whether *RAC2* haplotypes also affected disease expression in RRMS and CD by testing for correlations between haplotypes and age at disease onset. This latter information was available for 325 and 147 RRMS and CD patients, respectively. As shown in table 4, no association was observed between age at onset in CD and *RAC2* haplotypes. Conversely, in the case of MS, haplotypes in group B were associated with a significantly earlier presentation of symptoms, whereas the opposite was observed for haplotypes in cluster A2 (table 4). The same results were obtained after accounting for the presence of the

Table 3. Association of *RAC2* Haplotypes with Susceptibility to RRMS and CD.

Haplogroup	Frequency		OR (95% CI)	*P*	OR (95% CI)[a]	*P*[a]
	RRMS (n = 387)	Controls (n = 335)				
A1	0.270	0.289	0.91 (0.71–1.13)	0.426	0.91 (0.71–1.14)	0.416
A2	0.390	0.424	0.85 (0.69–1.07)	0.166	0.85 (0.68–1.07)	0.161
B	0.340	287	1.30 (1.04–1.64)	0.024	1.31 (1.05–1.66)	0.022
	CD (n = 149)	Controls (n = 164)				
A1	0.267	0.287	0.90 (0.64–1.30)	0.556	NP	NP
A2	384	0.439	0.78 (0.58–1.09)	0.136	NP	NP
B	0.349	0.274	1.41 (1.01–1.99)	0.048	NP	NP

NOTE.—CI, confidence interval; NP, not performed; OR, odds ratio.
[a] Adjusted for admixture.

*HLA-DRB*15* allele, a known risk factor for RRMS in Caucasians (supplementary table S5, Supplementary Material online).

Discussion

RAC2 is a protein expressed in the hematopoietic cell lineage and is involved in signal transduction in various cellular processes, such as chemotaxis, cytoskeletal rearrangement, cellular differentiation, and proliferation (Heasman and Ridley 2008). Production of proinflammatory cytokines and cysteine cysteine (CC) chemokines, secretion of reactive oxygen species by neutrophils, and cyclooxygenase-2 (COX-2) production by macrophages are also modulated by RAC2 (Heasman and Ridley 2008). Thus, RAC2 is a key player in the inflammation process, acting at different levels, and being involved in multiple mechanisms of immunity.

The state of *RAC2* expression influences the ability of this gene to trigger inflammatory responses. Some pathogens, in fact, downregulate *RAC2* transcription to escape cellular innate immune response (i.e., respiratory burst activation), facilitating their intracellular survival (Carlyon et al. 2002). Similarly, both bacterial and viral pathogens were shown to have the ability to target the protein product of *RAC2* and alter its activity (Janardhan et al. 2004; Chung et al. 2010; Groves et al. 2010). Among these pathogens, the SIV- and HIV-encoded Nef proteins interact with RAC2 to alter T-cell function (Janardhan et al. 2004). Notably, recent data indicate a significant association between chromosome microsatellite markers in 22q12-13 (where RAC2 is located) and resistance to HIV infection in HIV exposed but uninfected individuals (Kanari et al. 2005). An accurate analysis of this region allowed the identification of *RAC2* gene SNPs that were significantly associated with the resistance phenotype displayed by exposed uninfected individuals and with the development of particularly potent HIV-specific cell-mediated immunity (Kanary Y, Hakata Y, et al. 2012).

Table 4. Association of *RAC2* Haplotypes with Age at Onset in RRMS and IBD.

Disease	Haplogroup	BETA	*P*
RRMS (n = 325)	A1	0.382	0.602
	A2	1.551	0.029
	B	−1.519	0.025
CD (n = 147)	A1	−0.137	0.940
	A2	−1.558	0.349
	B	1.578	0.326

NOTE.—BETA is the regression coefficient.

In general, these observations indicate that RAC2 may be involved in host–pathogen genetic conflicts; consequently, the gene may represent a target of natural selection and harbor variants that affect the susceptibility to infectious diseases or other immunological phenotypes in humans. Nonetheless, inspection of available databases revealed no polymorphic amino acid variation segregating at detectable frequency in human populations, suggesting that functional polymorphisms in *RAC2*, if present, may occur within regulatory noncoding regions. We therefore exploited interspecific genetic diversity data to identify gene regions that may harbor functional noncoding sequences and analyzed their evolutionary pattern in three human populations. Our data indicate that the genomic portion covering the 3′ gene region displays extremely high nucleotide diversity, an excess of intermediate frequency alleles, and a higher level of within-species diversity compared with interspecific divergence, as assessed by the MLHKA test.

All these features strongly suggest the action of balancing selection. In particular, analysis of haplotype genealogy indicated the presence of three clades, which is consistent with a model of multiallelic balancing selection. This observation is in line with values of SFS-based statistics (Tajima's *D* and Fu and Li's *F** and *D** statistics), which are not strikingly positive, as the skew towards intermediate frequency variants tends to be less marked in a multiallelic selection model than in the case of biallelic selection. Calculation of the TMRCA for the $RAC2_{3'}$ haplotype genealogy yielded and estimate of 2.54 My, a coalescence time deeper than those estimated for most neutrally evolving autosomal human loci, which range from 0.8 to 1.5 My (Garrigan and Hammer 2006). Overall, these data strongly suggest that long-term balancing selection has maintained distinct functional alleles in *RAC2*. Inspection of polymorphisms located along the major branches of the genealogy indicated that several variants in DNaseI hypersensitive sites divide clade A and B haplotypes. In particular, variants rs933222, rs933221, rs4821610, and rs4821609 occur within a 600 bp portion located downstream the transcription end site; this region displays histone marks associated with enhancers (H3K4Me1 and H3K27Ac) in lymphoblastoid cell lines, suggesting that one or a combination of these SNPs alter RAC2 transcriptional activity and represent

functional variants. Experimental analyses will be required to evaluate this possibility. Similarly, rs9798725 (immediately downstream the transcription end site) occurs within a sequence conserved in mammals and separates the two major clades of the phylogeny.

It is worth mentioning that evolutionary scenarios different from balancing selection might account for the results we obtained. One alternative possibility is that the high nucleotide diversity we observed at the *RAC2*$_{3'}$ gene region is the result of a relaxation of selective constraint (which allows accumulation of new mutations). Yet, the region was selected because of the presence of DNaseI hypersensitive sites and sequence elements conserved across mammals and primates. Thus, relaxation of functional constraints would have occurred recently, with the only involvement of human populations. Moreover, nucleotide diversity in the region is extremely high, ranking above the 98th percentile in the distribution of reference windows. These latter are randomly drawn from resequenced genes and most of them cover intronic regions, where functional constraints are expected to be relatively relaxed; thus, we believe that the high diversity at *RAC2*$_{3'}$ is more likely to result from a selective process. Indeed, an alternative explanation to balancing selection is diversifying selection, which refers to a situation whereby genotypes are favored merely because they are different and therefore results in the maintenance of multiple alleles. This is an interesting possibility that might fit the evolutionary history of a gene involved in immune response that, as mentioned above, is targeted by different pathogen species. Yet, the molecular signatures of balancing and diversifying selection are difficult to disentangle, and population genetics analyses only provide a snapshot of a dynamic evolutionary process, making it difficult to precisely determine the underlying selective regime. For example, although F_{ST} was not exceptionally high, clear differences can be appreciated in the distribution of *RAC2* haplotypes across ethnic groups, suggesting that locally exerted selective pressures might have been acting during a more recent time frame.

From a biological perspective, one possibility is that the three major *RAC2* haplotypes are differentially active in distinct cell types or modulate gene expression in response to diverse stimuli. A similar hypothesis has been proposed to explain long-term balancing selection in the promoter region of major histocompatibility complex class II genes (Cowell et al. 1998; Beaty et al. 1999; Loisel et al. 2006). This view is consistent with the recent demonstration (Dimas et al. 2009) that the majority of variants affecting gene regulation in the human genome are cell-type specific, and that cell-specific regulatory elements tend to localize relatively distant from the transcription start site. An alternative possibility is that distinct alleles may have been selected to prevent the down-modulation or misregulation of *RAC2* transcription exerted by pathogens (Carlyon et al. 2002). Under these scenarios, the selective pressure acting on RAC2 is expected to be pathogen driven. Yet, other authors (Ferrer-Admetlla et al. 2008) have recently suggested that the maintenance of genetic diversity at immune response loci may result from the need to balance protection against invading pathogens with maintenance of self-tolerance. Indeed, our data indicate that haplotypes in *RAC2* associate with predisposition to MS and CD. Specifically, haplotypes belonging to clade B were significantly more common in patients compared with controls, and in RRMS patients, the presence of B haplotypes correlated with an earlier presentation of disease symptoms. Growing evidences in recent years have indicated that a portion of susceptibility alleles is shared among two or more autoimmune conditions (reviewed in Zenewicz et al. 2010). This observation has been interpreted in terms of common disease pathways being involved in the pathogenesis of autoimmune disorders and partially explains the cooccurrence of distinct autoimmune conditions in patients and families. Indeed, several studies have indicated that some degree of comorbidity is observed between MS and CD in affected individuals and their family members (Weng et al. 2007; Nielsen et al. 2008; Langer-Gould et al. 2010). Therefore, our association of the same haplotype with susceptibility to both MS and CD can be regarded as a strong confirmation of the causal role of RAC2 variants in the pathogenesis of autoimmune diseases.

As mentioned above, RAC2 is thought to have a central role in the regulation of RICD, a mechanism that contributes to the maintenance of CD4+ T-cell tolerance. Physiologically, RICD occurs more often with self rather that foreign antigens and is therefore considered as a "propriocidal" form of cell death that limits T-cell expansion in the presence of persistent antigen (reviewed in Snow et al. 2010). In this light, gene products involved in RICD can be regarded as excellent candidates to carry variants associated with autoimmune diseases. Indeed, polymorphisms in Fas and FasL have previously been associated with susceptibility to MS (Zayas et al. 2001; van Veen et al. 2002; Kantarci et al. 2004; Lucas et al. 2004), and a recent genome-wide association study for primary sclerosing cholangitis (Melum et al. 2011), an autoimmune conditions that often occurs in IBD patients, identified an SNP close to the *BCL2L11* gene (also known as BIM), another key player in the elicitation of RICD (Snow et al. 2010). Therefore, our data are in agreement with the conundrum whereby distinct susceptibility variants for a given trait may occur in genes that participate in a shared molecular pathway.

Despite the fact that our data indicate *RAC2* as a susceptibility gene for autoimmune diseases, it remains to be evaluated whether the predisposition to autoimmunity can be regarded as a selective pressure during the evolutionary history of humans. In fact, Plenge (2010) reported that the prevalence of several autoimmune disorders, including MS, is increasing in human communities (at least in developed countries) but their contribution to population fitness throughout human history, although unknown, can hardly be regarded as comparable to that of infectious diseases. Therefore, we tend to favor a model whereby balancing selection in the *RAC2* regulatory 3′ gene region is pathogen driven, and the resulting maintenance of susceptibility alleles for CD and MS can be regarded as a by-product of long-term

selection (reviewed in Sironi and Clerici 2010). Indeed, pathogen-driven balancing selection has previously been shown to maintain a subset of susceptibility alleles for IBD in human populations (Fumagalli, Pozzali, et al. 2009).

In summary, data herein show that integration of different approaches can provide valuable insight into the location of putative functional variants and on haplotype structure, which in turn can be applied to association studies. We describe for the first time an association between specific haplotypes of the *RAC2* gene and autoimmunity. Therapeutic approaches aimed at inhibiting or, at least, decreasing *RAC2* expression and/or activity could be beneficial in these patients. Statins were shown to interfere with RAC2 activity, limiting both T-cell activation and COX-2 macrophages production (Brinkkoetter et al. 2006; Habib et al. 2007). Notably, recent results indicated that atorvastatin, a statin, has beneficial antiinflammatory effects in CD patients (Grip et al. 2008).

Therefore, these results, although needing validation in bigger cohorts, suggest that RAC2 plays a potentially important role in the immunopathogenesis of autoimmune disease, possibly as a consequence of the ability of this gene to regulate T lymphocytes activity. Modulation of *RAC2* activity might be a novel potential therapeutic target in patients with autoimmune diseases.

Supplementary Material

Supplementary tables 1–5 are available at *Molecular Biology and Evolution* online (http://www.mbe.oxfordjournals.org/).

Acknowledgments

M.C. is supported by grants from The Eli and Edythe Broad Foundation (IBD-0294), Istituto Superiore di Sanita' "Programma Nazionale di Ricerca sull' AIDS", the EMPRO and AVIP EC WP6 Projects, the nGIN EC WP7 Project, the Japan Health Science Foundation, 2008 Ricerca Finalizzata (Italian Ministry of Health), 2008 Ricerca Corrente (Italian Ministry of Health), Progetto FIRB RETI: Rete Italiana Chimica Farmaceutica CHEM-PROFARMA-NET (RBPR05NWWC), and Fondazione CARIPLO.

References

Asthana S, Schmidt S, Sunyaev S. 2005. A limited role for balancing selection. *Trends Genet.* 21:30–32.

Balding DJ. 2006. A tutorial on statistical methods for population association studies. *Nat Rev Genet.* 7:781–791.

Bandelt HJ, Forster P, Rohl A. 1999. Median-joining networks for inferring intraspecific phylogenies. *Mol Biol Evol.* 16:37–48.

Barreiro LB, Quintana-Murci L. 2010. From evolutionary genetics to human immunology: how selection shapes host defence genes. *Nat Rev Genet.* 11:17–30.

Beaty JS, Sukiennicki TL, Nepom GT. 1999. Allelic variation in transcription modulates MHC class II expression and function. *Microbes Infect.* 1:919–927.

Benvenuti F, Hugues S, Walmsley M, Ruf S, Fetler L, Popoff M, Tybulewicz VL, Amigorena S. 2004. Requirement of Rac1 and Rac2 expression by mature dendritic cells for T cell priming. *Science* 305:1150–1153.

Boyle AP, Davis S, Shulha HP, Meltzer P, Margulies EH, Weng Z, Furey TS, Crawford GE. 2008. High-resolution mapping and characterization of open chromatin across the genome. *Cell* 132:311–322.

Brinkkoetter PT, Gottmann U, Schulte J, van der Woude FJ, Braun C, Yard BA. 2006. Atorvastatin interferes with activation of human CD4(+) T cells via inhibition of small guanosine triphosphatase (GTPase) activity and caspase-independent apoptosis. *Clin Exp Immunol.* 146:524–532.

Carlyon JA, Chan WT, Galan J, Roos D, Fikrig E. 2002. Repression of rac2 mRNA expression by anaplasma phagocytophila is essential to the inhibition of superoxide production and bacterial proliferation. *J Immunol.* 169:7009–7018.

Charlesworth D. 2006. Balancing selection and its effects on sequences in nearby genome regions. *PLoS Genet.* 2:e64.

Chung KJ, Cho EJ, Kim MK, et al. (11 co-authors). 2010. RtxA1-induced expression of the small GTPase Rac2 plays a key role in the pathogenicity of Vibrio vulnificus. *J Infect Dis.* 201:97–105.

Cowell LG, Kepler TB, Janitz M, Lauster R, Mitchison NA. 1998. The distribution of variation in regulatory gene segments, as present in MHC class II promoters. *Genome Res.* 8:124–134.

Croker BA, Tarlinton DM, Cluse LA, Tuxen AJ, Light A, Yang FC, Williams DA, Roberts AW. 2002. The Rac2 guanosine triphosphatase regulates B lymphocyte antigen receptor responses and chemotaxis and is required for establishment of B-1a and marginal zone B lymphocytes. *J Immunol.* 168:3376–3386.

Decoursey TE, Ligeti E. 2005. Regulation and termination of NADPH oxidase activity. *Cell Mol Life Sci.* 62:2173–2193.

Devlin B, Roeder K, Bacanu SA. 2001. Unbiased methods for population-based association studies. *Genet Epidemiol.* 21:273–284.

Dimas AS, Deutsch S, Stranger BE, et al. (11 co-authors). 2009. Common regulatory variation impacts gene expression in a cell type-dependent manner. *Science* 325:1246–1250.

Enoch MA, Shen PH, Xu K, Hodgkinson C, Goldman D. 2006. Using ancestry-informative markers to define populations and detect population stratification. *J Psychopharmacol.* 20:19–26.

Evanno G, Regnaut S, Goudet J. 2005. Detecting the number of clusters of individuals using the software STRUCTURE: a simulation study. *Mol Ecol.* 14:2611–2620.

Falush D, Stephens M, Pritchard JK. 2003. Inference of population structure using multilocus genotype data: linked loci and correlated allele frequencies. *Genetics* 164:1567–1587.

Ferrer-Admetlla A, Bosch E, Sikora M, et al. (11 co-authors). 2008. Balancing selection is the main force shaping the evolution of innate immunity genes. *J Immunol.* 181:1315–1322.

Fu YX, Li WH. 1993. Statistical tests of neutrality of mutations. *Genetics* 133:693–709.

Fumagalli M, Cagliani R, Pozzoli U, Riva S, Comi GP, Menozzi G, Bresolin N, Sironi M. 2009. Widespread balancing selection and pathogen-driven selection at blood group antigen genes. *Genome Res.* 19:199–212.

Fumagalli M, Pozzoli U, Cagliani R, Comi GP, Riva S, Clerici M, Bresolin N, Sironi M. 2009. Parasites represent a major selective force for interleukin genes and shape the genetic predisposition to autoimmune conditions. *J Exp Med.* 206:1395–1408.

Garrigan D, Hammer MF. 2006. Reconstructing human origins in the genomic era. *Nat Rev Genet.* 7:669–680.

Glazko GV, Nei M. 2003. Estimation of divergence times for major lineages of primate species. *Mol Biol Evol.* 20:424–434.

Gonzalez JR, Armengol L, Sole X, Guino E, Mercader JM, Estivill X, Moreno V. 2007. SNPassoc: an R package to perform whole genome association studies. *Bioinformatics* 23:644–645.

Griffiths RC, Tavare S. 1994. Sampling theory for neutral alleles in a varying environment. *Philos Trans R Soc Lond B Biol Sci.* 344:403–410.

Griffiths RC, Tavare S. 1995. Unrooted genealogical tree probabilities in the infinitely-many-sites model. *Math Biosci.* 127:77–98.

Grip O, Janciauskiene S, Bredberg A. 2008. Use of atorvastatin as an anti-inflammatory treatment in Crohn's disease. *Br J Pharmacol.* 155:1085–1092.

Groves E, Rittinger K, Amstutz M, Berry S, Holden DW, Cornelis GR, Caron E. 2010. Sequestering of Rac by the Yersinia effector YopO blocks Fcgamma receptor-mediated phagocytosis. *J Biol Chem.* 285:4087–4098.

Habib A, Shamseddeen I, Nasrallah MS, Antoun TA, Nemer G, Bertoglio J, Badreddine R, Badr KF. 2007. Modulation of COX-2 expression by statins in human monocytic cells. *FASEB J.* 21: 1665–1674.

Heasman SJ, Ridley AJ. 2008. Mammalian rho GTPases: new insights into their functions from in vivo studies. *Nat Rev Mol Cell Biol.* 9:690–701.

Hudson RR. 2002. Generating samples under a Wright-Fisher neutral model of genetic variation. *Bioinformatics* 18:337–338.

Hurst LD. 2009. Fundamental concepts in genetics: genetics and the understanding of selection. *Nat Rev Genet.* 10:83–93.

Janardhan A, Swigut T, Hill B, Myers MP, Skowronski J. 2004. HIV-1 Nef binds the DOCK2-ELMO1 complex to activate rac and inhibit lymphocyte chemotaxis. *PLoS Biol.* 2:E6.

Kalinowski ST. 2004. Counting alleles with rarefaction: private alleles and hierarchical sampling designs. *Conserv Genet.* 5:539–543.

Kanari Y, Clerici M, Abe H, et al. (12 co-authors). 2005. Genotypes at chromosome 22q12-13 are associated with HIV-1-exposed but uninfected status in Italians. *AIDS.* 19:1015–1024.

Kanari Y, Hakata Y, Wichukchinda N, et al. (23 co-authors). Forthcoming 2012. High-level *Rac2* expression associated with intron polymorphisms restricts HIV-1 replication in human cells. *J Clin Invest.*

Kantarci OH, Hebrink DD, Achenbach SJ, Atkinson EJ, de Andrade M, McMurray CT, Weinshenker BG. 2004. CD95 polymorphisms are associated with susceptibility to MS in women. A population-based study of CD95 and CD95L in MS. *J Neuroimmunol.* 146:162–170.

Kim C, Dinauer MC. 2001. Rac2 is an essential regulator of neutrophil nicotinamide adenine dinucleotide phosphate oxidase activation in response to specific signaling pathways. *J Immunol.* 166:1223–1232.

Kimura M. 1983. The neutral theory of molecular evolution. Cambridge: Cambridge University Press.

Knaus UG, Heyworth PG, Evans T, Curnutte JT, Bokoch GM. 1991. Regulation of phagocyte oxygen radical production by the GTP-binding protein Rac 2. *Science* 254:1512–1515.

Langer-Gould A, Albers KB, Van Den Eeden SK, Nelson LM. 2010. Autoimmune diseases prior to the diagnosis of multiple sclerosis: a population-based case-control study. *Mult Scler.* 16:855–861.

Lennard-Jones JE. 1989. Classification of inflammatory bowel disease. *Scand J Gastroenterol Suppl.* 170:2–6.

Li B, Yu H, Zheng W, Voll R, Na S, Roberts AW, Williams DA, Davis RJ, Ghosh S, Flavell RA. 2000. Role of the guanosine triphosphatase Rac2 in T helper 1 cell differentiation. *Science* 288:2219–2222.

Li S, Yamauchi A, Marchal CC, Molitoris JK, Quilliam LA, Dinauer MC. 2002. Chemoattractant-stimulated Rac activation in wild-type and Rac2-deficient murine neutrophils: preferential activation of Rac2 and Rac2 gene dosage effect on neutrophil functions. *J Immunol.* 169:5043–5051.

Loisel DA, Rockman MV, Wray GA, Altmann J, Alberts SC. 2006. Ancient polymorphism and functional variation in the primate MHC-DQA1 5′ cis-regulatory region. *Proc Natl Acad Sci U S A.* 103:16331–16336.

Lucas M, Zayas MD, De Costa AF, Solano F, Chadli A, Dinca L, Izquierdo G. 2004. A study of promoter and intronic markers of Apol/Fas gene and the interaction with Fas ligand in relapsing multiple sclerosis. *Eur Neurol.* 52:12–17.

Marth GT, Czabarka E, Murvai J, Sherry ST. 2004. The allele frequency spectrum in genome-wide human variation data reveals signals of differential demographic history in three large world populations. *Genetics* 166:351–372.

McDonald WI, Compston A, Edan G, et al. (16 co-authors). 2001. Recommended diagnostic criteria for multiple sclerosis: guidelines from the international panel on the diagnosis of multiple sclerosis. *Ann Neurol.* 50:121–127.

Melum E, Franke A, Schramm C, et al. (43 co-authors). 2011. Genome-wide association analysis in primary sclerosing cholangitis identifies two non-HLA susceptibility loci. *Nat Genet.* 43:17–19.

Nei M, Li WH. 1979. Mathematical model for studying genetic variation in terms of restriction endonucleases. *Proc Natl Acad Sci U S A.* 76:5269–5273.

Nielsen NM, Frisch M, Rostgaard K, Wohlfahrt J, Hjalgrim H, Koch-Henriksen N, Melbye M, Westergaard T. 2008. Autoimmune diseases in patients with multiple sclerosis and their first-degree relatives: a nationwide cohort study in Denmark. *Mult Scler.* 14:823–829.

Plenge R. 2010. GWASs and the age of human as the model organism for autoimmune genetic research. *Genome Biol.* 11:212.

Pritchard JK, Stephens M, Donnelly P. 2000. Inference of population structure using multilocus genotype data. *Genetics* 155:945–959.

Purcell S, Neale B, Todd-Brown K, et al. (11 co-authors). 2007. PLINK: a tool set for whole-genome association and population-based linkage analyses. *Am J Hum Genet.* 81:559–575.

Ramaswamy M, Dumont C, Cruz AC, Muppidi JR, Gomez TS, Billadeau DD, Tybulewicz VL, Siegel RM. 2007. Cutting edge: Rac GTPases sensitize activated T cells to die via Fas. *J Immunol.* 179:6384–6388.

Schaffner SF, Foo C, Gabriel S, Reich D, Daly MJ, Altshuler D. 2005. Calibrating a coalescent simulation of human genome sequence variation. *Genome Res.* 15:1576–1583.

Sironi M, Clerici M. 2010. The hygiene hypothesis: an evolutionary perspective. *Microbes Infect.* 12:421–427.

Sironi M, Menozzi G, Comi GP, Cagliani R, Bresolin N, Pozzoli U. 2005. Analysis of intronic conserved elements indicates that functional complexity might represent a major source of negative selection on non-coding sequences. *Hum Mol Genet.* 14:2533–2546.

Snow AL, Pandiyan P, Zheng L, Krummey SM, Lenardo MJ. 2010. The power and the promise of restimulation-induced cell death in human immune diseases. *Immunol Rev.* 236:68–82.

Stephens M, Scheet P. 2005. Accounting for decay of linkage disequilibrium in haplotype inference and missing-data imputation. *Am J Hum Genet.* 76:449–462.

Stephens M, Smith NJ, Donnelly P. 2001. A new statistical method for haplotype reconstruction from population data. *Am J Hum Genet.* 68:978–989.

Tajima F. 1989. Statistical method for testing the neutral mutation hypothesis by DNA polymorphism. *Genetics* 123:585–595.

Thornton K. 2003. Libsequence: a C++ class library for evolutionary genetic analysis. *Bioinformatics* 19:2325–2327.

Tishkoff SA, Verrelli BC. 2003. Patterns of human genetic diversity: implications for human evolutionary history and disease. *Annu Rev Genomics Hum Genet.* 4:293–340.

van Veen T, Kalkers NF, Crusius JB, van Winsen L, Barkhof F, Jongen PJ, Pena AS, Polman CH, Uitdehaag BM. 2002. The FAS-670 polymorphism influences susceptibility to multiple sclerosis. *J Neuroimmunol.* 128:95–100.

Voight BF, Adams AM, Frisse LA, Qian Y, Hudson RR, Di Rienzo A. 2005. Interrogating multiple aspects of variation in a full resequencing data set to infer human population size changes. *Proc Natl Acad Sci U S A.* 102:18508–18513.

Watterson GA. 1975. On the number of segregating sites in genetical models without recombination. *Theor Popul Biol.* 7:256–276.

Weng X, Liu L, Barcellos LF, Allison JE, Herrinton LJ. 2007. Clustering of inflammatory bowel disease with immune mediated diseases among members of a northern California-managed care organization. *Am J Gastroenterol.* 102:1429–1435.

Wright S. 1950. Genetical structure of populations. *Nature* 166:247–249.

Wright SI, Charlesworth B. 2004. The HKA test revisited: a maximum-likelihood-ratio test of the standard neutral model. *Genetics* 168:1071–1076.

Yu H, Leitenberg D, Li B, Flavell RA. 2001. Deficiency of small GTPase Rac2 affects T cell activation. *J Exp Med.* 194:915–926.

Zayas MD, Lucas M, Solano F, Fernandez-Perez MJ, Izquierdo G. 2001. Association of a CA repeat polymorphism upstream of the Fas ligand gene with multiple sclerosis. *J Neuroimmunol.* 116:238–241.

Zenewicz LA, Abraham C, Flavell RA, Cho JH. 2010. Unraveling the genetics of autoimmunity. *Cell* 140:791–797.

Attenuated Food Anticipatory Activity and Abnormal Circadian Locomotor Rhythms in *Rgs16* Knockdown Mice

Naoto Hayasaka[1]*, Kazuyuki Aoki[2], Saori Kinoshita[3], Shoutaroh Yamaguchi[2], John K. Wakefield[4¤a], Sachiyo Tsuji-Kawahara[3], Kazumasa Horikawa[2], Hiroshi Ikegami[5], Shigeharu Wakana[6], Takamichi Murakami[7], Ram Ramabhadran[4¤b], Masaaki Miyazawa[3], Shigenobu Shibata[2]

1 Department of Anatomy and Neurobiology, Kinki University School of Medicine, Osaka-Sayama, Osaka, Japan, **2** Department of Physiology and Pharmacology, School of Advanced Science and Engineering, Waseda University, Shinjuku-ku, Tokyo, Japan, **3** Department of Immunology, Kinki University School of Medicine, Osaka-Sayama, Osaka, Japan, **4** Tranzyme Pharma, Durham, North Carolina, United States of America, **5** Department of Endocrinology, Metabolism and Disease, Kinki University School of Medicine, Osaka-Sayama, Osaka, Japan, **6** Technology and Development Team for Mouse Phenotype Analysis: Japan Mouse Clinic, RIKEN Bioresource Center, Tsukuba, Ibaraki, Japan, **7** Department of Radiology, Kinki University School of Medicine, Osaka-Sayama, Osaka, Japan

Abstract

Regulators of G protein signaling (RGS) are a multi-functional protein family, which functions in part as GTPase-activating proteins (GAPs) of G protein α-subunits to terminate G protein signaling. Previous studies have demonstrated that the *Rgs16* transcripts exhibit robust circadian rhythms both in the suprachiasmatic nucleus (SCN), the master circadian light-entrainable oscillator (LEO) of the hypothalamus, and in the liver. To investigate the role of RGS16 in the circadian clock *in vivo*, we generated two independent transgenic mouse lines using lentiviral vectors expressing short hairpin RNA (shRNA) targeting the *Rgs16* mRNA. The knockdown mice demonstrated significantly shorter free-running period of locomotor activity rhythms and reduced total activity as compared to the wild-type siblings. In addition, when feeding was restricted during the daytime, food-entrainable oscillator (FEO)-driven elevated food-anticipatory activity (FAA) observed prior to the scheduled feeding time was significantly attenuated in the knockdown mice. Whereas the restricted feeding phase-advanced the rhythmic expression of the *Per2* clock gene in liver and thalamus in the wild-type animals, the above phase shift was not observed in the knockdown mice. This is the first *in vivo* demonstration that a common regulator of G protein signaling is involved in the two separate, but interactive circadian timing systems, LEO and FEO. The present study also suggests that liver and/or thalamus regulate the food-entrained circadian behavior through G protein-mediated signal transduction pathway(s).

Citation: Hayasaka N, Aoki K, Kinoshita S, Yamaguchi S, Wakefield JK, et al. (2011) Attenuated Food Anticipatory Activity and Abnormal Circadian Locomotor Rhythms in *Rgs16* Knockdown Mice. PLoS ONE 6(3): e17655. doi:10.1371/journal.pone.0017655

Editor: Paul Bartell, Pennsylvania State University, United States of America

Received January 12, 2011; **Accepted** February 4, 2011; **Published** March 9, 2011

Funding: This study was supported by Grant-in-Aid for Scientific Research: No. 19590235 and 21590264 from the Japan Society for the Promotion of Science, Grants-in-Aid from the Ministry of Education, Culture, Sports, Science and Technology of Japan including the High-Tech Research Center and Anti-aging Center grants, those from the Ministry of Health, Labor and Welfare of Japan for Research on HIV/AIDS, and those from the Japan Health Sciences Foundation. The funders had no role in study design, data collection and analysis, decision to publish, or preparation of the manuscript.

Competing Interests: Authors include employees at Tranzyme Pharma and have an affiliation to Tranzyme Pharma using the material TranzVector for the study. This does not alter the authors' adherence to all the PLoS ONE policies on sharing data and materials.

* E-mail: hayasaka@med.kindai.ac.jp

¤a Current address: Thermo Scientific/Open Biosystems, Huntsville, Alabama, United States of America
¤b Current address: Integrated Systems Toxicology Division, NHEERL, ORD, United States Environmental Protection Agency, Research Triangle Park, North Carolina, United States of America

Introduction

The circadian timing system in mammals exerts control over a wide range of physiology and behavior, including daily environmental changes, the circadian system can be reset by external time cues (Zeitgeber) such as light and metabolic correlates of feeding [1–3]. Two separate, but coupled oscillators, LEO and FEO, are involved in circadian system(s) in mammals. Whereas the master LEO is located in the SCN of the hypothalamus [4,5], localization of the FEO(s) still remains to be determined [6–8]. An output of a putative FEO is FAA, which can be assessed by restricted feeding (RF), daily limiting food availability to a restricted time window. SCN lesion studies demonstrated that FEO-driven FAA persists without the LEO, suggesting that FEO resides outside of the SCN [6,9,10]. It is also reported that FEO dominates LEO under RF in the entrainment of activity phase [4]. Moreover, disruption of the known circadian clock genes resulted in mostly partial or little alterations of FAA [11]. These data suggest that the FEO, which functions under limited nutrient availability, is a dominant circadian oscillator independent of LEO.

To elucidate molecular machinery driving circadian clock(s) in mammals, a list of candidate circadian clock/clock-controlled genes have been identified by microarray [8,12,13]. Among these was *Rgs16*, a member of RGS family. RGS proteins regulate G protein-coupled receptor (GPCR)-mediated signaling by negatively or positively interacting with downstream effectors [14]. In the brain, *Rgs16* is predominantly expressed in the SCN and thalamus [15,16]. RGS16 exhibits robust circadian rhythms both in the SCN and in liver with its peak at 4–6 (zeitgeber time, ZT4-6) and 8–10 (ZT8-10) hours after light-on, respectively, suggesting that

RGS16 is involved in the central and peripheral circadian clocks and/or their outputs [16]. Interestingly, a previous study demonstrated that *Rgs16* expression in liver was up-regulated during fasting and rapidly down-regulated by re-feeding [17]. In addition, expression of *Rgs16* in liver was restricted to periportal hepatocytes, the predominant locations of gluconeogenesis and lipolysis [17]. Considering that a number of GPCR ligands including vasoactive intestinal peptide (VIP; [18]), glutamate [19,20], melatonin [21,22], orexin [23,24] and ghrelin [25,26] have been implicated in the central or peripheral circadian clocks, these data raise the possibility that RGS proteins function in the circadian systems by modulating signaling through as yet unknown GPCR/GPCR ligand(s).

Here, to elucidate the possible role of RGS16 in the circadian clock *in vivo*, we generated two independent knockdown (KD) mouse lines using lentiviral vectors expressing two separate short hairpin RNAs (shRNAs) targeting the *Rge16* mRNA.

Results

Generation of the *Rgs16* knockdown mice

We designed different shRNAs against different regions of *Rgs16*. Each shRNA expression vectors was transfected into NIH3T3 cell line and levels of the *Rgs16* mRNA were quantified by quantitative RT-PCR (qPCR). The two shRNAs silencing endogenous *Rgs16* mRNA with the greatest efficiency (#41 and #53) were selected for producing two independent transgenic mouse lines (Fig. S2). We then produced separate high-titer lentiviral vector lots encoding the two shRNA expression cassettes as well as the GFP protein, and introduced them into fertilized one-cell stage mouse embryos by microinjection into the perivitelline space [27,28]. The transgenic mice were selected by detecting GFP expression and the presence of the transgene confirmed by PCR-based genotyping.

Expression of the *Rgs16* mRNA in the KD and wild-type brain and liver

We first examined the spacio-temporal expression patterns of the *Rgs16* mRNA in brain and liver of the KD and wild-type (WT) mice by *in situ* hybridization (ISH) and quantitative PCR (qPCR). In the WT brain, predominant expression of *Rgs16* was observed in the SCN, and at a lower level in thalamus (Fig. 1A). We also confirmed that *Rgs16* transcription exhibits robust circadian rhythms in the SCN (Fig. 1B). As shown in Fig. 1C, average *Rgs16* expression level was reduced the KD SCN (Fig. 1C). In the WT liver, robust circadian rhythms were observed peaking at ZT11 (Fig. 1D, $F = 21.7$, $P<0.001$). In the KD liver, average *Rgs16* expression level was reduced, and circadian changes were weakened (Fig. 1D, $F = 6.06$, $P<0.05$) relative to the controls ($F = 21.7$, $P<0.001$). In thalamus, no daily expression rhythms were observed in both WT ($F = 0.65$, $P>0.05$) and KD ($F = 0.36$, $P>0.05$) mice (Fig. 1E). The average expression level of *Rgs16* in the KD thalamus was lower than that of WT control, however, the knockdown efficiency was lower than that in liver (Fig. 1D, E).

Free-running period of locomotor activity rhythm was shorter in the KD mice

To study the possible involvement of RGS16 in the central circadian clock, we examined locomotor activity rhythms of the KD and control mice. Wheel-running activities of individual mice were monitored under 12 hr light and 12 hr dark (LD) and constant dark (DD) conditions (Fig. 2A, B). In DD, The KD mice showed an average free-running period significantly shorter than

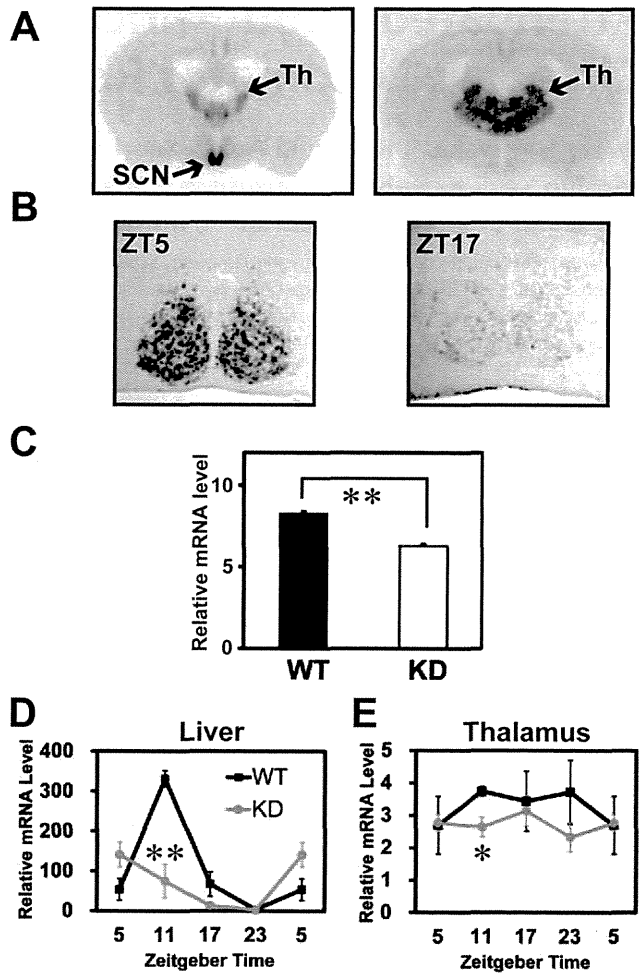

Figure 1. Spatial and temporal expression patterns of the *Rgs16* mRNA in brain and its reduction in the KD mice. A, B, *in situ* hybridization performed on brain sections. **A,** Specific and intense signals were observed in the SCN and thalamus (Th). **B,** Diurnal rhythms of the *Rgs16* transcript were observed in the SCN. **C,** ISH quantification of the *Rgs16* mRNA in the KD and WT SCN (n = 8 each) at ZT5. $^{**}P<0.01$ vs. WT (Student's *t*-test). **D,** Expression of *Rgs16* in the KD and WT liver observed by qPCR. $^{**}P<0.01$ vs. WT (Student's *t*-test). ##, $P<0.01$ circadian gene expression profile by 2-way ANOVA (WT vs. KD mice; n = 3–4). **E,** Expression of *Rgs16* in thalamus of the KD and WT mice (n = 3–4). $^{*}P<0.05$ vs. WT.
doi:10.1371/journal.pone.0017655.g001

that of the controls (23.84±0.05 hr in WT vs. 23.45±0.07 hr in KD, $P<0.01$, Fig. 2C). After locomotor activity rhythms were assessed, brains were sampled at ZT5 from individual KD and WT mice and quantitative ISH was performed on the brain sections. Average *Rgs16* mRNA level in the SCN was significantly decreased in the KD mice relative to controls (Fig. 1C).

Total amount of locomotor activity was reduced in the *Rgs16* KD mice

We next compared total amount of locomotor activity of the *Rgs16* KD mice with that of controls. Total activity counts were assessed by an infrared sensor of KD and WT mice averaged every 30 minutes. The average activity of the KD mice was significantly lower than that of the controls regardless of day or night (Fig. 3A, B), whereas averaged day/night ratio of locomotor activity was comparable between the two genotypes (Fig. 3C).